Chinese Chemical Letters 35 (2024) 108533

Contents lists available at ScienceDirect

Chinese Chemical Letters

journal homepage: www.elsevier.com/locate/cclet

Review of MXenes as a component in smart textiles and an adsorbent for textile wastewater remediation

Kaniz Farhana[a,*], Kumaran Kadirgama[b,c], Abu Shadate Faisal Mahamude[d], Rajan Jose[e,f]

[a] Department of Apparel Engineering, Bangladesh University of Textiles, Dhaka 1208, Bangladesh
[b] Faculty of Mechanical and Automotive Engineering Technology, Universiti Malaysia Pahang, 26600 Pekan, Pahang, Malaysia
[c] Center of Automotive Engineering, Universiti Malaysia Pahang, Malaysia
[d] College of Engineering, Universiti Malaysia Pahang, 26300 Gambang, Pahang, Malaysia
[e] Faculty of Industrial Sciences & Technology, Universiti Malaysia Pahang, 26300 Kuantan, Malaysia
[f] Center of Intelligent Materials, Universiti Malaysia Pahang, 26300 Kuantan, Malaysia

ARTICLE INFO

Article history:
Received 27 November 2022
Revised 9 February 2023
Accepted 29 April 2023
Available online 1 May 2023

Keywords:
Textile fibers
Industrial wastewater treatment
MAX phases
Hybrid electrodes
Adsorption

ABSTRACT

Two-dimensional (2D) MXenes have emerged as an archetypical layered material combining the properties of an organic-inorganic hybrid offering materials sustainability for a range of applications. Their surface functional groups and the associated chemical properties' tailorability through functionalizing MXenes with other materials as well as hydrophilicity and high conductivity enable them to be the best successor for various applications in textile industries, especially in the advancement of smart textiles and remediation of textile wastewater. MXene-based textile composite performs superb smartness in high-performance wearables as well as in the reduction of textile dyes from wastewater. This article critically reviews the significance of MXenes in two sectors of the textile industry. Firstly, we review the improvement of textile raw materials such as fiber, yarn, and fabric by using MXene as electrodes in supercapacitors, pressure sensors. Secondly, we review advancements in the removal of dyes from textile wastewater utilizing MXene as an absorbent by the adsorption process. MXene-based textiles demonstrated superior strength through the strong bonding between MXene and textile structures as well as the treatment of adsorbate by adsorbent (MXene in the adsorption process). We identify critical gaps for further research to enable their real-life applications.

© 2023 Published by Elsevier B.V. on behalf of Chinese Chemical Society and Institute of Materia Medica, Chinese Academy of Medical Sciences.

1. Introduction

Textiles rank among the top five fundamental demands of human life and are the most indispensable for civilized life. Over eighty billion pieces of cloth are consumed every year globally for a wide variety of needs in addition to the fundamental clothing, such as electronic devices for a range of applications including energy conversion and storage, healthcare, sensing, automotive, protective, sports [1–5]. The revolution of textiles over centuries has enabled much control of the fabric production process for developing multipurpose cloths with durability, washable, wearability, fashionable, and reusability [6–10]. Smart or intelligent textiles are the next generation in the evolution of textiles owing to the incessant demands on miniaturization and multifunctionality [11–15]. These functionalized textiles can be upgraded extensively by using nanomaterials as nanofibers or nanocomposite substrates [16–19]. Nanofinishing [20–22] and nanocoating [23–25] processes can provide various functional or high-performance characteristics to textile substrates. Dip-coating, plasma polymerization, layer-by-layer coating, sol-gel, and spray coating are the most relevant nanocoating approaches to preparing smart textiles [26–28]. Further, the emergence of two-dimensional (2D) materials such as graphene, MXenes, transition metal dichalcogenides, etc. with superior properties to their 3D analogs has also contributed to enhancing the functionalities of smart textiles [29,30].

Among the 2D materials, MXenes [31,32] are a family of early transition eco-friendly metal carbides and carbonitrides by Gogotsi *et al.* [33,34] and are designed to be appropriate for a wide range of applications, from medical and optoelectronics owing to their promising chemical, physical and mechanical attributes [35–40]. Significant investments in this material for various technologies have raised a growing academic interest as can be seen from the exponential growth of science and engineering research papers (Fig. 1A) besides the emergence of a market sector (Fig. 1B). One would easily observe the increasing attention on this material by

* Corresponding author.
E-mail address: kaniz.farhana@ae.butex.edu.bd (K. Farhana).

https://doi.org/10.1016/j.cclet.2023.108533
1001-8417/© 2023 Published by Elsevier B.V. on behalf of Chinese Chemical Society and Institute of Materia Medica, Chinese Academy of Medical Sciences.

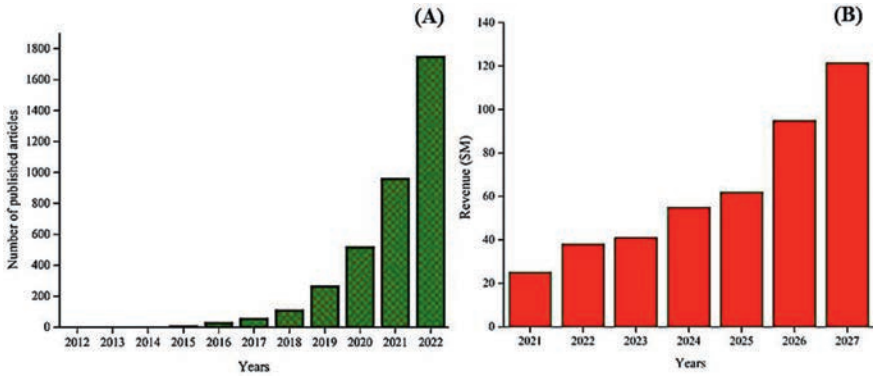

Fig. 1. Status of MXene nanomaterials: (A) Progression of published articles on MXenes from 2012 to 2022 (last ten years). The data was obtained from Web of Science database using the keywords "MXene nanomaterials" OR "smart textiles" OR "textile wastewater" on 31 Dec 2022. (B) Global market scenario of MXene nanomaterials. The data was obtained from https://www.industryarc.com/Report/20088/MXene-market.html on 31 December 2022.

the academic community from Fig. 1A. Correspondingly, the MXene market has been projected to grow from $26.4 million in 2022 to $121.5 million in 2027 with a CAGR of 29.24%. A summary of the structure and properties of MXenes is in the next section (Section 2). In the textile-constructed systems, the size of the MXene flake is a key feature for their functionalization as it impacts significantly on the morphology of corresponding yarns as well as the characteristics of the final textile. Generally, large flakes in the long distribution range from ~100 nm to ~10 μm could be prepared using the MILD method while the small flake of size range of ~0.1–100 nm using more sonication and density gradient centrifugation [41–43]. Small-sized MXene flakes are coated in textile fibers (cotton) by penetrating the yarn and interstice. On the other hand, large MXene covers the surface of yarn which results in electrical conductivity improvement compared to textile materials coated with small MXene flakes. These occurred owing to the irregularity fractions and increased interfacial resistance of small flakes [44,45]. Besides, the size of MXene flakes is also significant for MXene-based electrodes in the case of electrochemical performance. Moreover, the dispersion of MXene flakes into the proper solution is another paramount factor for functionalization to enhance the performance of smart textiles. Current studies reported that MXene is quite dispersible in a variety of solvents such as water, dimethylformamide (DMF), ethanol, dimethyl sulfoxide (DMSO) [46–48]. MXene performs good dispersion properties along with the formation termination groups with similar polarities to interact with textile materials. In this regard, the stability of dispersed MXene flakes in the solvents is also highly required to show its capabilities in textile materials [49–51].

Nevertheless, the textile industry is one of the most polluting entities; this issue must be compulsorily addressed for sustainability and to eliminate or minimize waste or their proper management [52]. In the case of the textile industry, oily wastewater is one of the main waste streams generated, which in many cases has been addressed using membrane technology [53–55]. Recently, halloysite nanotubes (Hal and polydopamine (PDA) were used with MXene following fabrication to form Hal@MXene-PDA composite membranes *via* vacuum filtration for ultra-high oil-in-water separation [56]. Besides, there are efficient processes for poisonous metal removal from wastewater that have transformational influences to alleviate freshwater shortages. Adsorption is one of the most promising purification techniques because of its simple, cost-effective, and excellent efficiency in a conditioned environment. In this context, MXene-based nanocomposites have emerged as a promising adsorbent to remediate toxic metals from wastewater owing to their hydrophilicity, large surface area, activated metallic hydroxide sites, enormous electron availability, and substantial adsorption ability [57–60]. The continuous progress of MXene nanostructure or nanocomposite for wastewater treatment is necessary to update timely and to emphasize deeply to apply toxic metal remediation concerned with the environmental path, characterization approaches, advantages, and limitations of MXene using the adsorption process [61–65].

In this article, we review the suitability of MXene in smart textiles and textile wastewater remediation and provide essential insights on human health, sports, entertainment, and textile wastewater treatment to the safe surrounding environment. The application of MXene in the textile industry has been analyzed for this study, which included both empirical and experimental research. The process flow of analysis, the discussion of smart textiles and MXene, MXene in textile materials, and MXene in textile wastewater treatment have all been adequately recapped one after the other. Firstly, portrayed with the introduction part includes general information about textile smart clothing and the remediation of textile dyes from wastewater. Most importantly narrated about MXene in this section. Secondly, the research methodology was prepared by making a research flowchart of the complete works of this current study. Thirdly, the performance of MXene nanomaterials in textile raw materials (Fiber/yarn/fabric) for new-generation clothing or smart clothing has been observed neatly. Fourthly, the process and remediation of dyes from textile wastewater by using MXene as an absorbent has been investigated precisely. And lastly, the incorporation and performance of MXene in the textile zone have been discussed scientifically.

2. Structure and properties of MXenes

The chemical structure of MXene can be expressed generally as $M_{n+1}X_nT_x$; where T stands for the surface functional groups such as fluorine (F), chlorine (Cl), hydroxyl (OH), and oxygen (O); and X symbolizes the number of surface termination groups [66,67]. Analogous to the synthesis of 2D graphene from 3D graphite, 2D MXenes are synthesized from their parent MAX phase. MAX phase is a certain atomic layer of hexagonal layered structure; trio transition metal nitrides or carbides with a general formula $M_{n+1}AX_n$; where M is the early transition metal such as Ti, Cr, V, Mo, Zr, Hf, Ta, Nb, Sc, W; X denotes nitrogen and/or carbide and A is the interleaved layer between M and X; n is ranged from 1 to 3 [68,69], as shown in Fig. 2A [70–72]. In the $M_{n+1}AX_n$ structure, two chemical bonding pairs exist such as M-A and M-X, where the latter is chemically more stable than the former and offers metallic or covalent, or ionic properties [33,73]. Therefore, M-A bonding in the MAX phase can be relatively easily detached by selective etching of interleaved A layer without interrupting M-X bonds as portrayed

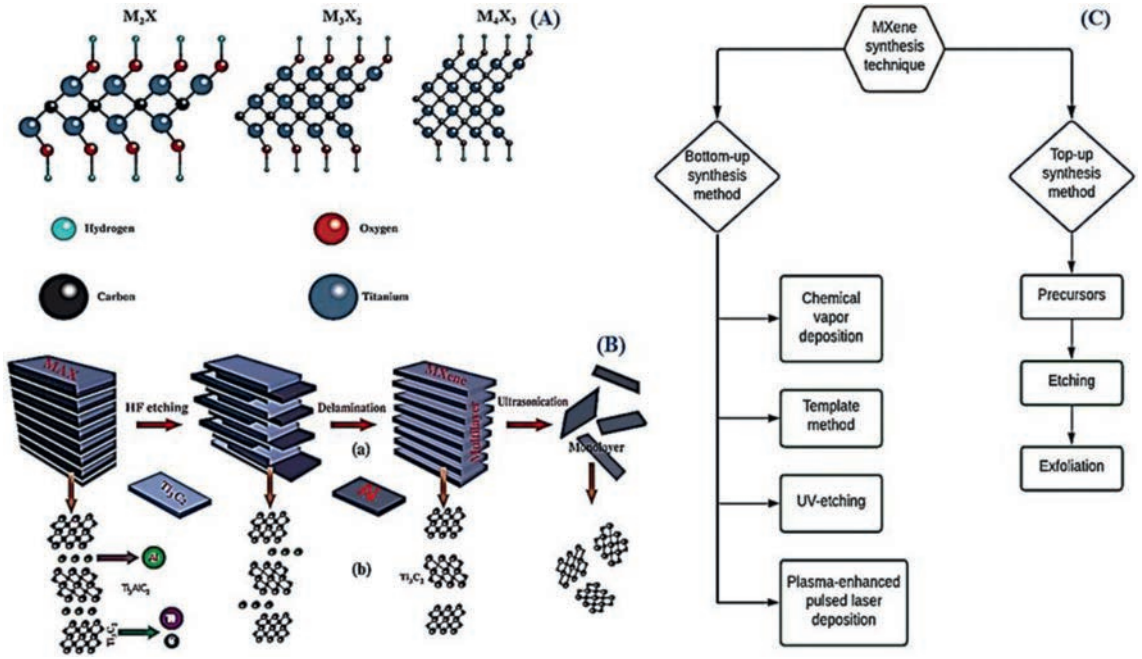

Fig. 2. (A) Crystal arrangement of different layered of MXenes with surface functional groups as hydroxyl (OH). Reproduced with permission [76]. Copyright 2021, Elsevier. (B) (a) Schematic illustration of Ti_3AlC_2 MAX phase to the monolayer of Ti_3C_2 MXene transformation and (b) chemical structure of Ti_3AlC_2 MAX (312) to Ti_3C_2 MXene following the etching process. Reproduced with permission [72]. Copyright 2021, Elsevier. (C) synthesis techniques of MXene preparation. Reproduced with permission [76]. Copyright 2021, Elsevier.

in Fig. 2B. Generally, MXene is synthesized by following top-down and bottom-up techniques as shown in Fig. 2C [67,74-76]. The top-down approach provides MXene from their parent precursors using selective etching with hydrofluoric (HF) acid at >55 °C [71,77]. Exfoliation is essential to convert multilayers MXene into single nanosheets; sonication or shaking are the most convenient approaches [78]. On the other hand, bottom-up methods, as depicted in Fig. 2C, produce excellent quality and ultrafine MXene films [79]. The first MXene synthesized had a formula $Ti_3C_2T_X$ by selective etching of the Al layer from the Ti_3AlC_2 MAX phase precursor using hydrofluoric acid, the T_X refers to various surface functional groups such as -O, -OH, -F, -C introduced during the chemical processing stage [67,80]. Etching is performed with acids, hence MXene is illustrated with these surface functional groups [81,82]. A large number of synthesis techniques have been applied to produce MXenes in various studies such as *in-situ* growth [83], the hydrothermal method [84], heterojunction [85], intensive layer delamination [86].

Varied choices of M and X ions in the MXene structure give them a unique choice of property tailoring *via* compositional variation. Characteristically, as produced MXene is a highly electrically conductive material of conductivity ~9.1 S/cm [87–89]. However, the electrical conductivity depends on the synthesis process; the electrical conductivity of individual flakes of MXene have as high as $(4.6 \pm 1.1) \times 10^3$ S/cm, which could be enhanced over 2×10^4 S/cm *via* appropriate compositional tailoring [90–92]. Besides, $Ti_3C_2T_X$ offers desirable electrochemical properties and high volumetric capacitance (1274 F/cm^3 at 10 mV/s), which makes them excellent electrochemical capacitor electrodes and sensors [19,93-101]. MXene has sufficient termination groups (-OH, -O, or -F) obtained on the surface of MXene at the time of synthesis [102,103] which is considered the main factor of their mechanical characteristics [104]. However, these functional groups can alter their property-owning to thermal treatments and the alkylation process [105,106]. Flexibility and structural firmness are two additional remarkable mechanical characteristics of MXene flakes owing to the surface stacking character [107]. The atomic layers in the chemical structure of MXene are also another influential factor to have impressive mechanical properties; as consequence, the rigidness and tensile strength of MXene ($M_{n+1}X_n$) enhance with decreasing n [108,109]. Due to these surface functional groups, $Ti_3C_2T_X$ offers much higher Youngs modulus (330 ± 30 G and tensile strength (17.3 ± 1.6 GPa), which are higher than those of graphene oxide and reduced graphene oxide [110–112].

Due to their high electrical conductivity, and mechanical and electrochemical properties, MXenes are intriguing for producing wearable electronics (e-textiles) that may be worn like normal clothes [113,114]. MXenes present a compelling case to produce conductive yarns using a simple and scalable manufacturing process and have mechanical properties that make them durable enough to withstand the wear and tear experienced by normal textiles [2,115,116]. Moreover, MXene nanocomposite exhibits superb thermal stability and plays a vital role to prevent polymer degradation due to its excellent physical barrier effect [117,118]. Recently, a method that combines the flexible chemistry of MXene with commercial cellulose-based yarns to produce promising electrical and electrochemical capabilities are developed [44,119,120], which are designed for 3D knitted supercapacitors to improve the performance of a knit construction with long yarn electrodes. Because of their rich adjustable surface terminations and chemical hydrophilicity, MXenes have enticing prospects for sensors, energy storage, and shielding applications in portable, wearable, and flexible smart fabrics [41,121,122]. As an example of the multifarious property of MXenes, direct printing onto the textile is required to make wearable electronics on a larger scale. Hence, a basic approach is to formulate conductive inkjet printable, additive-free aqueous MXene inks for direct printing [123]. MXene-based electrical ducts and micro-supercapacitors (MSCs) were printed on textile materials by controlling the geometry of the nozzle for higher-resolution inkjet printing. The textile-based MSCs performed areal capacitance improvement up to 294 mF/cm^2 in eclipsing established printed MXene-based MSCs and inkjet-printed MSCs using

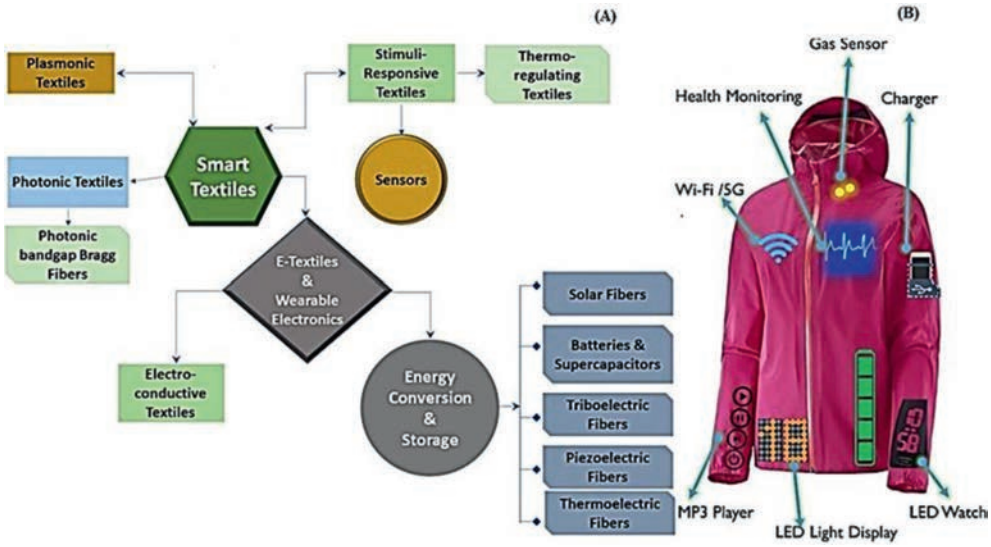

Fig. 3. (A) Classification of smart and intelligent textiles. (B) Smart wearable textile with numerous applications. Reconstructed following the References [126,131,132]. Copyright 2019, Elsevier; Copyright 2021, Washington Post; Copyright 2018, Berlin Fashion Week.

different 2D nanoparticles thereby providing a vital step toward growing the purposeful capability of conductive inks and simplifying the fabrication of wearable textile-primarily based electronics. Fiber and yarn-based supercapacitors are now dominating this field and have performed well in yarn lengths < 4 cm; however, when the yarn length increases, the performance begins to sway due to increased resistance [124,125].

3. Definition and types of smart textiles

The raising development of innovative technology and science has also made a drastic change in textiles. Moreover, it can be modified according to environmental changes by providing responsive specific characteristics and functions. The emerging part of textiles that are capable to sense external changes and reacting to them by special attributes of textile substrate, called smart or intelligent textiles. Therefore, textile substrates are not solely confined to warm retaining, protective and fashionable attributes. Furthermore, it can be altered according to environmental changes by providing responsive specific characteristics and functions which can be made by endorsing intelligent fiber, unique design in yarn and fabric, or technological advancement in modification.

Generally, e-textile is mainly segmented into three parts such as sensors, actuators, and control units [126]; smart textiles are categorized as (i) passive smart textiles which sense only external stimuli [27]; (ii) active smart textiles which sense reactions to the circumferential environmental condition [127]; (iii) smart and intelligent textiles which sense, react, and adapt their attribute to the external situation [127,128]. Broadly, e-textiles and wearable electronics, thermo-regulating textiles, stimuli-responsive textiles, plasmonic textiles, and photonic textiles with individual branches are mainly mentioned as smart and intelligent textiles as illustrated in Fig. 3A [27,126-132]. All kinds of e-textile can be passive or active smart materials. E-textile and wearable textiles are prepared primarily based on the breathability, flexibility, resiliency, stability, and bending properties of textile materials. Also, other electronic properties of textiles can be attained *via* the incorporation of nanomaterials such as graphene and carbon nanotube (CNT) into it [133,134]. The intersection of nanoelectronics with textiles suggests unique behavior for high-performance applications such as supercapacitors, electrostatic power generators, textiles batteries. Photonic textiles are integrated with polymeric optical fibers, light-emitting diodes, photoluminescent polymer-coated fibers, sensors, and thermochromic dye-coated yarns for changing the characteristics by altering emission frequency, colors, and design of emitted lights [135]. Bragg fibers are one type of photonic fiber; prepared by making solid and hollow-core ringed by sporadic dielectric nanolayers with low and high reflective indexes [136]. Plasmonic textiles were prepared by conformal deposition of metal nanoparticles by immersion of cotton fabric into the solution encompassed with nanoparticles (Ag, Au, and Pt) and followed by an *in-situ* synthesis system. Various colors in the fabric were created due to the diverse size and shapes of nanoparticles that were presented on the surface of cotton fabrics [137]. Of late, gold-coated optical plasmonic fiber-based sensors have been used in smart textiles to detect dew creation, and this had been offered by Esmaeilzadeh *et al.* [138]. Generally, stimuli-responsive polymers are used in smart textiles to change their properties with surrounding environmental stimuli-deviation including light-responsive polymers, piezo-responsive polymers, pH-responsive polymers, thermal-responsive polymers, and moisture-responsive polymers. These kinds of polymers functionalize enormous attributes to smart textiles such as esthetic look, comfort, fantasy design with varied colors, wound tracking, smart wetting behavior, drug delivery system, and safeguard against extreme weather [139,140]. Currently, the application of nanotechnology in stimuli-responsive textiles exhibits better performance such as nanofiber-based shape memory polymer which can return to a permanent shape from a temporary shape by the effect of extraneous stimuli [141]. Finally, thermo-regulating textiles are prepared by using phase change materials (PCMs) as they can change one physical condition to another to control the homogeneous temperature of textiles [142]. Microencapsulated is the most widely used PCMS to apply on textile substrates for the formation of thermo-regulating smart textiles. Presently, nanomaterials such as CuO, TiO_2, Al_2O_3, and CNTs have been incorporated into PCMs to enhance thermal performance [143]. However, electrical insulation can be utilized to prevent electric shorts, shocks, and fires from occurring when wearing conductive materials. This electrical insulation of the conductive textiles can be achieved by enclosing the conducting elements in an electrically insulating layer using techniques like core spinning or tubular intarsia knitting, or by encasing them in a water-resistant polymer [144]. Intelligent clothing

made of these above techniques has been portrayed in Fig. 3B that could be used for multifunctional purposes.

4. MXene in textile materials (fiber/yarn/fabric)

4.1. Synthesis of textiles with MXene

Due to the void structure of fiber/yarn assembly, textile substrate shows breathability; besides, textile substrates are flexible, resilient, and stable under various conditions [145,146]. These superiorities of textile materials can be employed beneficially for diverse applications. Besides, the above attributes play a significant role to achieve electrochemical functionalities through the incorporation of nanomaterials with improved electrical conductivity, tensile strength, sensing, electrocatalytic activity, and obvious suitability for smart electronics applications [22,147-149]. Along with other nanomaterials such as graphene, and carbon nanotube (CNT); MXene also has its proficiency in smart textiles [119].

Currently, there is little literature on MXene as a textile material and its effects on various textile materials such as cotton. Li *et al.* [150] reported a flexible piezoresistive pressure sensor based on MXene-textile fiber (cotton). The contact space between the MXene-textile wave and molybdenum (Mo) similarly interdigitated electrodes increases under external pressure (29–40 kPa) which leads to an improvement of current and decrement in resistance of MXene-textile film and MXene will get closer to a cotton textile fiber. This can make a more conductive route which leads to a decline in resistance of the MXene-textile film electrode and a great increment of current occurred. In another study on natural cotton fiber, Yan *et al.* [151] investigated the performances of polypyrrole-MXene coated textile-based supercapacitors (SCs) as rising flexible and wearable energy storage devices. Herein, MXene nanosheets were fabricated on the cotton textile, then PPy was accumulated on the surface of the MXene-based textile electrochemically to form MXene-PPy-textile electrode, and finally, supercapacitors decorated based on MXene-PPy textile electrode. The increased capacitance was demonstrated with mass-loading up to ~2 mg/mL. This happened owing to the hydroxyl group of cotton fiber and the good hydrophilicity and metallic conductivity of MXenes. In addition, Zheng *et al.* [152] studied reduced graphene oxide/MXene fabricated cotton fabric for multipurpose and reveal its the high-performance of it owing to the better inherent electrical conductivity of MXene, which can be related to the synergistic interactions between MXene and RGO sheets and more connected conductive networks. Moreover, cost-effective strain sensors, electromagnetic interference shielding, and electrochemical storages could be produced. Yin *et al.* [153] further investigated the electromagnetic interference shielding performance based on multi-structured PANI/MXene/CF fabric by a layer-by-layer approach and found excellent electromagnetic interference effectiveness and electrical conductivity. Due to superb electrostatic interaction and van der Waals forces between MXene, CF, and PANI. Uzun *et al.* [44] studied knitted and washable multifunctional MXene-coated cellulose yarn for next-generation textile-based electronics wearable devices and reported that small MXene (S-Ti_3C_2) flakes infiltrate between the individual fibers thereby producing 30–50 S/cm conductive yarn with excellent flexibility suitable for pressure and strain sensing. Besides, large MXene flakes (L-Ti_3C_2) dispersion had been used only on the surface to obtain MXene-coated conductive yarn. Due to the surface functional groups on MXene flakes, they are negatively charged and hydrophilic (-O, -OH, and -F). MXene flakes adhered to the surface of hydrophilic cotton yarns when they were dipped into negatively charged MXene dispersions. As a result, MXene flakes and cotton fibers developed powerful electrostatic interactions.

Wang *et al.* [154] conducted a hierarchical design based on MXene-cotton fabrics. Herein, the pre-treated cotton fabric had been immersed into the MXene suspension following silicon nanoparticles (SiNPs) to form MX@SiNPs cotton fabric. MXene-coated cotton performed excellent mechanical properties by creating inter-layer h-bonds, displaying numerous configurations of O–H bonds and various functional groups of individual MXenes platelets. Besides, Cao *et al.* [155] examined the tensile strength and electronic conductivity of 3D-printed smart fibers and textiles produced from MXene-reinforced cellulose nanofibril inks. In this study, 2,2,6,6-tetramethylpiperidin-1-oxylradical (TEMPO)-mediated oxidized cellulose nanofibril (TOCNFs) and MXene (Ti_3C_2) blended directly to TOCNFs/Ti_3C_2 ink that had been transformed into continuous TOCNFs/Ti_3C_2 fibers and textiles injecting into an ethanol coagulation bath using a facile 3D printer. TOCNFs/Ti_3C_2 fibers show significant responsiveness to multiple external stimuli (electrical/photonic/mechanical) owing to the sufficient functional groups, higher layer spacing between nanosheets and immense electrical conductivity.

Silk is another important natural source of textile fiber and just a little research with MXene being reported so far. Silk is a flexible and multifunctional textiles fiber and is promising for wearable electronics and portable device applications because of its innate flexibility and puros features. Liu *et al.* [156] synthesized the textile silk fiber with biomimetic leaf-like MXene/silver nanowire nanostructures for electromagnetic interference shielding efficiency improvement. Herein, the authors demonstrated a vacuum-assisted layer-by-layer assembly method to fabricate both 1D AgNWs and 2D MXene nanosheets to develop a deeply conductive biomimetic leaf-like nanostructure on porous textile by the synergistic effect that enables the developed textile exciting electrical conductivity, electromagnetic interference shielding, hugely sensitive humidity response, and extremely hydrophobicity. MXene resists oxidation to control AgNWs and increase the self-driven hydrophobicity of textiles by transforming functional groups. Another investigation was conducted by Hu *et al.* [157] who reported the performance of carbonized silk cloth (CSC) coated with MXene suspension as a flexible electrode for supercapacitors. MXene-coated CSCs (CSC@$Ti_3C_2T_x$) were quite flexible which allows them to be twisted and bent easily. This interesting and indispensable property generates the MXene-coated CSC fabric more convenient for flexible supercapacitor electrodes as MXenes show flexible mechanical and power sources.

The performance of MXene in man-made textile fibers is also taken into account to some extent, for instance, Li *et al.* [158] investigated the strategy to prepare high-performance textile-based electrodes with MXene flakes. Therefore, positively charged polyester fabric modified with polyethyleneimine (PEI) and negatively charged titanium carbide MXene nanosheets ($Ti_3C_2T_x$) were used to develop electrostatically self-assembled eminent conductive textile (MXene/PMFF). Afterward, conductive polymer polypyrrole (PPy) was placed on MXene/PMFF to produce PPy/MXene/PMFF supercapacitor electrode. The textile electrode's low charge transfer resistance, high capacitance, and improved cycling stability are made possible by PPy/MXene/PMFF, which also creates faster electrolyte ions diffusion paths and more active sites. In addition, Shao *et al.* [159] studied MXene-based polyester nanofibers as yarn electrodes in wearable storage devices such as yarn supercapacitors and batteries for powering smart textiles. The MXene NCY supercapacitor was performed with an immoderate capacitance but the rigorous areal energy density of power density. The availability of Ti, C, and O functional groups of MXenes improves the electro activeness of the supercapacitor.

Wang *et al.* [160] investigated the electromagnetic interference and joule heating performances of textile PET with MXene nanomaterials. Herein, MXene was incorporated on PET by the dip-

coating method to produce highly conductive hydrophobic and flexible yarn with notable electromagnetic interference shielding efficiency and joule heating performances as MXenes provide interfacial adhesion, increasing polar groups, as well as a wicking effect, was formed between them. In another study of synthesis with MXene, Wang *et al.* [161] studied helical core-sheath elastic yarn with an MXene sensing layer used as a humidity sensor or dual strain. Helical core-sheath yarn (CSY) was produced by a spinning trial machine using PU and PET filament. Helical conductive MXene-based core-sheath yarn (MCSY) prepared using MXene ink. Due to the high specific area of the yarn and the inherent hydrophilicity of the MXene sensing layer, the yarn sensor may also make a great humidity sensor.

In the case of other man-made fibers, Seyedin *et al.* [162] studied MXene-polyurethane (PU) composite and coaxial fibers with higher stretchability and conductivity for wearable strain-sensing textiles. Herein, MXene had been used in PYU textile fibers to obtain profoundly conducting stretchable MXene/PU composite fibers to enlarge sensing strain. MXene/PU demonstrated composite and coaxial fibers having highly conductive, morphological, sufficient mechanical, and stretchable properties that could be easily used in knitting for commercial purposes after evaluating various mechanical and electrical properties. Moreover, Luo *et al.* [163] studied MXene-based superhydrophobic and breathable smart textiles for multifunctional wearable sensing electronics. The textile fibers were intensely coated by the self-polymerization of dopamine to prepare PDA-textile following coating with MXene and PDMS to prepare PDA-MXene-PDMS fabricated textiles. PDMS makes the textile waterproof, and breathable and can protect the MXene layer from oxidation and degradation to increase the substantial stability of wearable smart textiles. Therefore, the assembly of MXene nanosheets onto the fiber surface to create a wrinkled structure is facilitated by the van der Waals force and hydrogen bonding when the textile is submerged in the MXene solution. Additionally, several large MXene sheets bridge and interconnect the adjoining fibers, enhancing the conductivity of the MXene network and the textile. The extraction of these studies has been summarized in Table S1 (Supporting information). Table S1 illustrates the schematic flow of MXene application in textiles materials such as fiber (Natural and man-made), yarn (Different kinds), and fabric (Knit and woven). It also mentions the other essential components such as polyimide (PI), polymer polypyrrole (PPy), polyethylene oxide (PEO), polyethyleneimine (PEI), isopropanol (IPA), acetic acid (AcOH), polyaniline (PANI), dimethyl sulfoxide (DMSO), aqueous ammonia ($NH_3 \cdot H_2O$), tetraethyl orthosilicate (TEOS), tempo oxidized cellulose nanofibrils (TOCNFs), polydopamine (PDA), polydimethylsiloxane (PDMS) used with MXene nanomaterial into textile materials to prepare smart and wearable textile for the next generation.

4.2. Process, equations, and performance of MXene on textiles

Based on the above literature (3.1 section), several methods have been employed to accomplish the textile composite integrated with MXene to make intelligent textiles using a wide range of chemical ingredients to work sharply. MXene can react with textiles using electrochemical equations to demonstrate the intelligence or smartness of textile materials, which is comprehended. Tables 1 and 2 summarize the results of this research. Here, Table 2 describes the incorporation procedure of MXene in textile materials. Most of the studies used a dip-coating approach to embody MXene nanomaterials into textile materials. Also, it discusses the integrated textile materials with MXene had been used as electrodes, pressure sensors, electromagnetic interference, multi-functional textiles, ink for 3D printing, and wearable sensing electronics. And finally, Table 2 signifies the unprecedented performance of MXene nanomaterials when organized for contemporary, smart, and wearable clothing for the new generation. Table 3 illustrates the computational equations that had been used in these studies to determine the performance of MXene-based textile materials numerically.

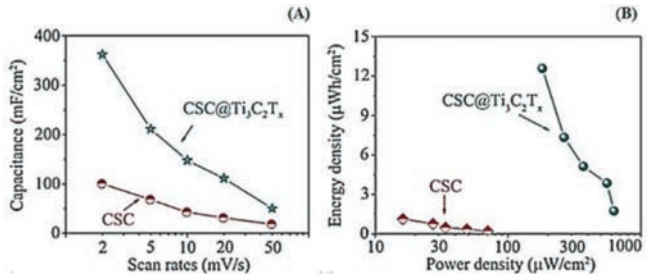

Fig. 4. Electrochemical performance of MXene-based textile electrode. Adapted with permission [157]. Copyright 2018, Elsevier.

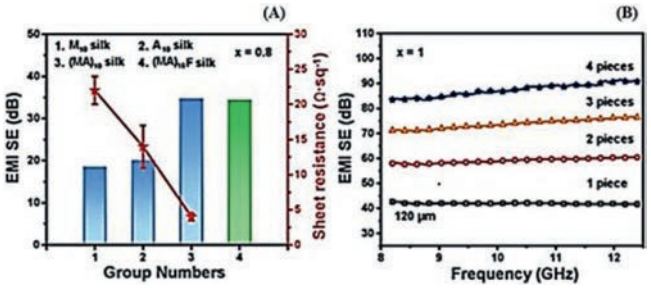

Fig. 5. Shielding effectiveness of textile materials. Adapted with permission [156]. Copyright 2019, Willy Online Library.

4.3. Analysis and findings of segments 4.1 and 4.2

Important findings of Sections 4.1 and 4.2 have been summarized in this part. MXene nanomaterials have already been incorporated into the textile field to fulfill the diversified requirements for next-generation clothing. In the case of smart textiles, MXene, and MXene-based nanomaterials have been utilized in next-generation textiles in varied forms and the performance of textiles has been exceptionally boosting up by using noble MXene as well. Due to the good chemical bonding and electrical conductivity property of MXene [88]; MXene-coated textiles perform excellent electrochemical behavior [44,151-153,157-159]. Hu *et al.* [157] reported the comparison status of electrochemical performance of CSC and CSC@$Ti_3C_2T_x$ electrodes as shown in Fig. 4. CSC@$Ti_3C_2T_x$ electrodes exhibited superior performance within a spectrum of 32 mF/cm^2 to 362 mF/cm^2 at the scan rate of 2 mV/s than CSC in electrochemical capacitance due to existing of $Ti_3C_2T_x$ nanomaterials (Fig. 4A). Also, CSC@$Ti_3C_2T_x$ portrayed a significantly higher power density compared to CSC (Fig. 4B). CSC@$Ti_3C_2T_x$ performed the energy density of 13 μWh/cm^2, concerning the power density of 181 μW/cm^2 at the scan rate of 2 mV/s. Besides, having good conductive properties, satisfactory mechanical flexibility, and remarkable surface group arrangement on the surface of MXene, MXene demonstrates excellent performance in electromagnetic interference shielding to human sweating and enhanced shielding effectiveness (SE) as well [44,152,153,156,160]. For instance, Liu *et al.* [156] inferred that MXene combined with silver nanowires on textile materials portrayed excellent performance of resistance of 2 ± 0.2 Ω/sq on electromagnetic interference shielding, and shielding effectiveness increased from 42 dB to 90 dB as portrayed in Fig. 5. Furthermore, MXene composite textiles also performed superb strain-induced behavior and textile strength for the exten-

Table 1
Performance of MXene in textile materials.

Incorporation process of MXene	Usages	Important findings	Ref.
Dip coating	Pressure sensor	Sensitivity obtained of 29–40 kPa and exceptional properties of the sensor such as voice recognition, finger touching, and bending were found	Li *et al.* [150]
Dip coating	Multifunctional textiles	Excellent electrical conductivity of ~1000 S/m; long-term structure and stability, better cycling and tunability performances for wearable intelligent clothing, highest electromagnetic interference shielding efficiency of ~90 dB, and personal heating applications	Wang *et al.* [160]
Dipping and drying	Supercapacitors	Capacitance increased by 343.20 F/g. and better flexibility was achieved	Yan *et al.* [151]
Dip coating	PANI/MXene/CF fabric for multi-purposes	An exceptional electromagnetic interference performance with high effectiveness of 26.0 dB; maximum electrical conductivity of 24.57 S/m and notable joule heating attribute; satisfactory flexibility, air permeability, processibility, and durability	Yin *et al.* [153]
Dip coating	Dual strain/humidity sensors	Good strain and humidity variation for humans as a wearable sensor; the sensor displayed 0.3% to 120% strain and 30% to 100% relative humidity (RH) detection performance	Wang *et al.* [161]
Single dip coating	Wearable sensing electronics	Notable hydrophobicity of about contact angle of ~151° and competent breathability; good recyclability and remarkable durability; and excellent strain sensing property	Luo *et al.* [163]
Two-step dipping and drying procedure	Yarn electrodes and supercapacitors	Excellent electrical conductivity of up to 440.3 ± 0.9 S/cm and remarkable in triboelectric energy harvesting electromagnetic interference shielding and heated fabrics	Uzun *et al.* [44]
Spray-coating and dip-coating	Multifunctional RMCs	Good electrochemical performance with higher capacitance, higher electromagnetic interference shielding, and joule heating properties. The maximum specific capacitance of 383.3 F/g was obtained	Zheng *et al.* [152]
Coating with immersing solution	Electrodes	Extremely good performance in high capacitance; rate capacity and cycling stability	Li *et al.* [158]
Coated with suspension	Supercapacitor electrodes	High capacitance of about high capacitance of 362 mF/cm^2, cyclability, flexibility performance	Hu *et al.* [157]
d-MXene and PEO nanofibers coated with PET	Supercapacitor yarn and energy storage device	Superb electrochemical capacitance of 18.39 mF/cm^2; ultra-high charge storage capability and drastic areal energy density of 0.38–0.67 μWh/cm^2 and power density of 0.09–0.39 mW/cm^2	Shao *et al.* [159]
Vacuum-assisted layer-by-layer assembly	Electromagnetic interference shielding	Unprecedented electromagnetic interference shielding efficiency of 54 dB; super hydrophobicity attribute; permeable and humidity responsive	Liu *et al.* [156]
Wet spinning process	MXene/PU composite and coaxial fibers	Composite shows notable conductive and stretchable properties; coaxial fibers exhibit superb sense strain performance of a high gage factor of ~12,900 and a big sensing strain of ~152%	Seyedin *et al.* [162]
Immersed in the suspension	Wearable sensor	Superb sensing performance of about $S_1 = 12.23\ kPa^{-1}$ sensitivity; excellent mechanical properties and great hydrophobic criteria	Wang *et al.* [154]
Direct mixing	3D-printed smart fibers and textiles	The case factor of sensitivity is 87.8 and 399.5 within the strain range of 4%–8% and 8%–10%, respectively; distinguished tensile strength and electrical conductivity	Cao *et al.* [155]

Table 2
Mathematical relations used in reviewed studies.

Equations	Remarks	Ref.
$R_{total} = R_{contact} + R_{film}$	To specify the resistance of the sensor	Li *et al.* [150]
$C = \frac{I\Delta t}{\Delta V}$	To determine the capacitance of the electrode	Li *et al.* [158], Shao *et al.* [159]
$E_D = \frac{1}{2} C_A \Delta V^2$	To evaluate the energy density of the electrode	Li *et al.* [158], Shao *et al.* [159]
$P_D = \frac{E_D}{\Delta t}$	To identify the power density of the electrode	Li *et al.* [158], Shao *et al.* [159]
$SE_T = SE_R + SE_A$	To evaluate the performance of electromagnetic interference shielding	Zheng *et al.* [152], Yin *et al.* [153]
$\frac{\Delta R}{R_0} = \frac{(R-R_0)}{R_0}$	To characterize the strain-sensing performance of the smart textile	Cao *et al.* [155] Wang *et al.* [161], Luo *et al.* [163]
$S = \frac{\Delta R}{\Delta RH}$	To interpret the sensitivity related to humidity sensing property	Wang *et al.* [161]

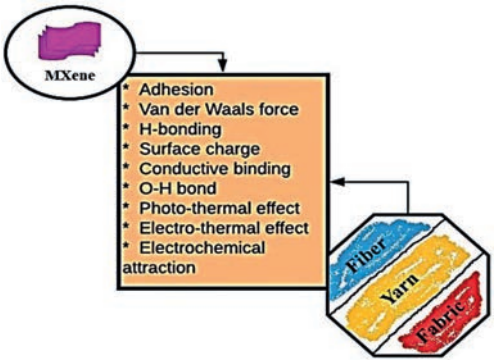

Fig. 6. Actions occurred between MXene and textile raw materials.

sibility of textile materials. Moreover, MXene-based textiles exhibited notable sensing performance. The presence of O–H or H-bond in MXene-based composite can react with textile materials as well as can monitor human body activity effectively. The photo-thermal, electro-thermal, and electrochemical interaction properties of MXene also play a vital role to adhere with textile materials to enhance its diverse functional properties such as sense, strength, elasticity, stiffness. Not only that, but the literature also stated possessing good flexibility properties in MXene; MXene depicted excellent repeated performance on applied bodies [154,161-163]. Reviewing and studying the literature, it has been figured out that diversified actions work between the textile raw materials and MXene nanomaterials to form an advanced composite for smart clothing such as van der Waals force, H-bonding, electrochemical interactions as illustrated in Fig. 6. Additionally, to obtain ac-

Table 3
Summary of process and performance of MXene in textile wastewater.

Adsorbents for treatment	Treated elements	Treatment process	Important outcomes	Ref.
MXene, phytic acid (PA), dimethyl sulfoxide (DMSO), sodium hydroxide (NaOH), hydrochloric acid (HCl)	Methylene blue (MB), Rhodamine B (RhB)	Dye adsorption	(1) Exhibited elevated adsorption capacities for MB and RhB dyes. At 12 h hydrothermal time, PA-MXene displayed the highest adsorption capacity of about 41.39 and 22.12 mg/g for MB RhB dyes respectively (2) Presented good adsorbent for wastewater treatment	Cai *et al.* [202]
MXene, humic acid (HA), HCl, sodium chloride (NaCl), NaOH	MB, Methyl orange (MO)	Dye adsorption and ultrasound assistance	(1) Exhibited a better adsorption capacity since MB removal rate increased more than 60% by MXene (2) Fast kinetics and good regeneration properties	Jun *et al.* [203]
MXene, potassium dichromate ($K_2Cr_2O_7$), NaOH, HCl, nitric acid (HNO_3), sodium bicarbonate ($NaHCO_3$), NaCl, and sodium sulfate (Na_2SO_4)	MO, chromium ions (Cr(VI))	Dye adsorption	(1) Excellent removal efficiencies; the highest removal efficiencies were 104 and 94.8 mg/g for Cr(VI) and MO, respectively (2) Notable adsorption capabilities demonstrated	Karthikeyan *et al.* [204]
MXene, sodium alginate (SA), PEI, trimethoxysilane (APTES), $K_2Cr_2O_7$, 1,5-diphenylcarbazide ($C_{13}H_{14}N_4O$), epichlorohydrin (ECH)	Cr(VI), Congo Red (CR)	Dye adsorption	(1) Remarkable adsorption capability for dyes of about 538.97 mg/g and 3568 mg/g towards Cr(VI) and Congo Red respectively (2) Also, firm against harmful bacteria	Feng *et al.* [205]
MXene, A100 MOF (MIL-53(Al)), HA, HCl, NaOH, NaCl, $CaCl_2$, and Na_2SO_4	MB and acid blue 80 (AB)	Dye adsorption	(1) Perform good electrostatic interaction with dyes (2) Displayed higher adsorption capacity for MB of about ~140 mg/g and AB of ~200 mg/g, respectively (3) Notable from an economic point of view	Jun *et al.* [206]
MXene, Fe_3O_4, magnetic nanoparticles (MNPs), hydrofluoric acid solution, tertiary butyl alcohol (TBA), *p*-benzoquinone (*p*-benz), hydrogen peroxide, dopamine hydrochloride, HCl, hydrazinium hydrate, ferric chloride tetrahydrate ($FeCl_2{\cdot}4H_2O$) and NaOH, ethyl alcohol (AR), DMSO	MB, CR, MO, and rhodamine B (RB),	Catalytic performance test	(1) Fast degradation of organic dyes obtained (2) Degradation efficiency might be greater than 97% (3) Good catalytic performance in cyclic usage	Cui *et al.* [207]
MXene nanosheets, CNTS, cotton fabric	Textile wastewater	Solar-driven interfacial water evaporation	(1) High optical absorption, photothermal conversion, water transport properties, high thermal insulating PS foam floater and sole cotton fibers-based water pathway, good water evaporation rate, and textile wastewater (2) Evaporation rate for water reaches 1.35 kg/m^2 and > 1.16 kg m^{-2} h^{-1} for textile wastewater (3) Potentially useful to treat textile wastewater	Wang *et al.* [208]
MXene, HCl, NaOH, hydrogen peroxide (H_2O_2), *t*-BuOH ($C_4H_{10}O$), potassium iodide (KI), potassium hydrogen phthalate ($C_8H_5KO_4$), and ammonium molybdate tetrahydrate ($H_{24}Mo_7N_6O_{24}{\cdot}4H_2O$)	MB and AB	Dye adsorption and ultrasonication	(1) More active sites for the adsorption process (2) Synergetic indices for removing MB ranged from 1.21 to 1.86, while those for removing AB ranged from 1.00 to 1.11 (3) MXene/us combined showed better performance	Jun *et al.* [209]

tual resultant data of electrodes, pressure sensor, supercapacitors, electromagnetic interference, wearable sensing electronics, multifunctional textiles; several studies calculated various mathematical expressions as tabulated in Table 2.

Application of MXene in smart textiles as; a sensor can be used in the wrist to record the radial artery pulse of the human heart as shown in Fig. 7A. Also, the sensor can be used in the throat to detect phonation and identify the changes in current frequency for diverse words of wearer speakers as presented in Fig. 7B [150]. MXene-based textile composite can be used in the human body's finger, elbow, and knee to monitor human body motions, physiological signals, personal thermal management, and temperature as portrayed in Figs. 7C-E. These MXene-based smart textiles exhibited superb variants of negative resistance and high sensitivity during any physical movement of the human body [152,163]. Uzun *et al.* [44], prepared MXene-based knitted pressure sensor buttons to sense varying levels of finger pressures and weights as displayed in Fig. 7F. Finally, the authors reported that the MXene-based knitted textile sensor is proficient to bear various levels of applied pressures and can also be utilized in practical life. Also, MXene-based textile portable electronics used as biomechanical sensors are impressive to detect finger-tapping human options as shown in Figs 7G; which demonstrated its potentiality in the wearable self-powered sensing approach [150,164]. In one study, Seyedin *et al.* [162] made a wearable strain-sensing knitted elbow sleeve using MXene with textiles fibers to record various movements of the human elbow as presented in Fig. 7H. This smart textile was also performed with an excellent magnitude of sensitivity at different strains and stability. Wireless body movement tracking systems were linked using this type of knitted elbow sleeve on the elbow of the human body for health, sports, and entertainment purposes. In another study, Liu *et al.* [156] prepared an MXene composite with textiles to make electromagnetic interference detect human humidity, especially sweating levels of humans as represented in Fig. 7I. They reported electromagnetic interference to determine remarkably sensitive humidity responses as resistance change increases for MXene-based textile composite with increasing levels of moisture in the human body. Besides, to monitor the motion of the human body, the researchers also used a back neck sensor made of MXene-based textiles such as Wang *et al.* [154] as shown

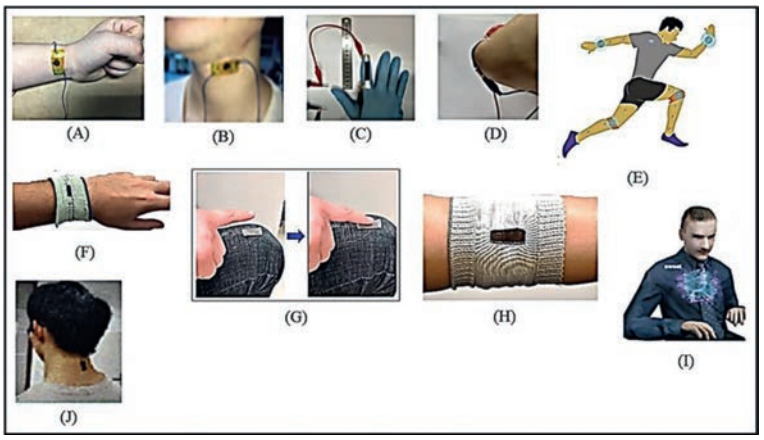

Fig. 7. Application of MXene-based smart textiles onto the human body. Reprinted with permission [44,150,152,154,156,162-164]. Copyright 2019, 2020, Willy Online Library; Copyright 2019, Royal Society of Chemistry; Copyright 2020, 2021, Elsevier.

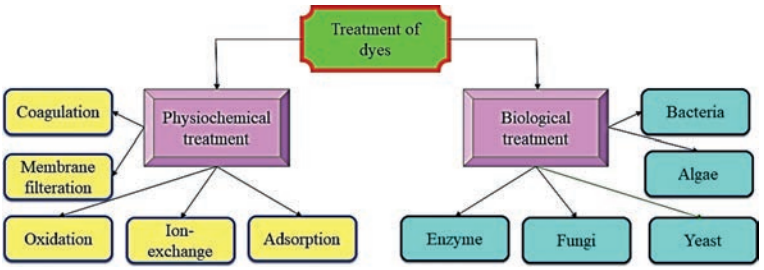

Fig. 8. Schematic presentation of dye remediation techniques from textile wastewater.

in Fig. 7J. The authors mentioned that back neck sensors produce more repeatable and durable signals persistent with the motion of the back neck.

5. MXene for textile wastewater treatment

5.1. Wastewater treatment by MXene

Physiochemical and biological treatments are the two fundamental techniques of textile dyes/wastewater remediation. Fig. 8 portrays the schematic diagram of textile wastewater treatment techniques [165,166]. Diverse branches of physiochemical methods are available to remediate textile wastewater such as coagulation [167], membrane filtration [168], oxidation [169], co-precipitations [170], ion exchange [171], reverse osmosis [172], adsorptions [173], and photodegradation [174]. All these conventional methods demonstrate low efficiency, high energy consumption, adverse outgrowth, and formation of inferior sludge [175,176]. Among these strategies, the adsorption system is the most widely employed technique to treat water the elimination of contaminants. Besides, this method is also simple to operate, has rapid kinetics, is efficient, has less toxic by-product formation, and demands low cost as well [177–180]. However, colloidal MXene flakes, on the other hand, degrade more safely in the environment when exposed to oxidation than pristine MXene flakes. This is because MXenes' metallic conductivity can be altered by the free electrons of transition metal atoms owning their tunable surface characteristics. This results in MXenes having a lower electrical conductivity and a preserved reactive interface due to their increased surface energy and moderate oxidation resistance in oxygenated conditions [181,182].

The unit cell of MXenes, which has a five-atomic sheet structure, is shaped like a hexagon. MXene has a width of 163 nm and a length of about 274 nm. The MXene layer height is 3 nm, with each layer being nominally 1 nm thick. However, it has been shown that the second layer is 1.6 nm thick. Most of the time, the "accordion" shape of MXene produced by the HF technique is adequate for the removal of colors from wastewater. The average lateral size (dimensional size) of 2D MXene is 219 ± 47 nm, making it effective for wastewater treatment as well as other purposes [183–185].

Of late, the adsorption technique has gained significant consideration for wastewater remediation as the process assists in excellent decolorization capacity for various dyes from textile wastewater [186,187]. An enormous number of adsorbents have been identified and discussed in the literature that is responsible to remediate dyes from textile wastewater such as activated carbon materials [188], zeolites [189], fly ash, wood, and agricultural waste [190], metal oxide [191], metal-organic frameworks [192], peat, and MXene [193,194]. The elemental criteria of an absorbent to treat wastewater are immense affinity, capability to separate dyes from wastewater, low cost, and superior rehabilitation ability [195,196].

Not only the dyes but also heavy metals such as Pb(II), Cr(VI), Hg(II), Cu(II), Sr, could be hazardous even in very tiny amounts, it is essential to remove them from water supplies. Metal removal can be performed in a variety of ways, but adsorption has been demonstrated to be the most efficient. Because the adsorption technique is incredibly simple, inexpensive, and effective even at very low metal concentrations. Based on some literature, Dong *et al.* [197] investigated the removal of Pb(II) using MXene/alginate composite and revealed an improved adsorption capacity of about 382.7 mg/g of Pb(II) from wastewater. Kong *et al.* [198] examined the remediation of Cr(II) utilizing MXene sheets and amino moieties (NH_2-$Ti_3C_2T_x$) compound synergistically by adsorbing. NH_2-$Ti_3C_2T_x$ maximizes the adsorption capacity up to 107.4 mg/g. In a different study, Shahzad *et al.* [199] synthesized magnetic carbide-based MXene nanocomposite (MGMX) and examined the elimination of mercuric ion (Hg(II)) from wastewater. The MGMX composite performed good evacuation of Hg(II) and the highest adsorption capacity of about 1128.41 mg/g was noticed. In the case

of Cu(II) heavy metal, Zhang *et al.* [200] prepared functionalized MXene (TN-EHL) nanosheets using enzymatic hydrolysis lignin and investigated the effective remediation of Cu(II) of wastewater. The maximum 49.96 mg/g adsorption capacity of Cu(II) removal was mentioned. Moreover, Jun *et al.* [201] explored the wastewater from hydraulic fracking including each natural and inorganic pollution using MXenes for the removal of radioactive nuclides consisting of Ba^{2+} and Sr^{2+}. MXene exhibited very rapid adsorption kinetics, achieving equilibrium within 1 h and reusability was brilliant over a minimum of 4 cycles. The study concluded that MXene appreciably eliminated Ba^{2+} and Sr^{2+} from sample fracking wastewater. There is a form of the electrolyte solution of single and double phases which will help them complete the process of removal.

Several works to treat dyes from textile wastewater have been reported such as Cai *et al.* [202] studied the synthesis of MXene-phytic acid (PA) nanocomposite to treat textile dyeing wastewater. Herein, MXene-PA nanocomposite was prepared using the facile hydrothermal method by selecting different hydrothermal times, varied samples were synthesized such as PA-MXene-0.5, PA-MXene-3, PA-MXene-6, PA-MXene-12, and PA-MXene-30. Before applying these nanocomposites to test, treatment had been done with dimethyl sulfoxide (DMSO). After that nanocomposite powder was placed into the methylene blue (MB), and rhodamine B (RhB) dye solutions to find out the adsorption capacity of the composites; followed by magnetic stirring in the dark of the dye solutions. To centrifuge the dye dispersion and obtain the supernatant is essential to investigate the absorbance. In another study, Jun *et al.* [203] investigated the adsorption mechanism and performance of dyes with the aid of ultrasound (US)-assisted MXene. Herein, 28 and 580 kHz ultrasound frequencies were used to dissipate MXene to treat textile wastewater. The samples of dye MB and Mo dispersion had been prepared with US-assisted MXene along with diverse specific conditions. US-assisted MXene obtained an enormous amount of oxygenated functional groups and scattering compared with pristine MXene which performed a great adsorption capacity than other conditions.

Karthikeyan *et al.* [204] investigated the removal of dyes from the aqueous systems by using 2D MXene nanosheets. Methyl orange (MO), and chromium ions (Cr(VI)) dispersions were employed to mix with MXene and stirred with a thermostat shaker. In other studies, Feng *et al.* [205] studied sodium alginate aerogel fabricated with MXene and polyethyleneimine to analyze the adsorption behavior for Cr(VI) and congo red (CR). Herein, the functionalized MXene-NH_2 was prepared by mixing MXene and APTES. Afterward, sodium alginate, PET, and ECH were added to MXene-NH_2 concentrations and placed for mechanical stirring; followed by washing and freeze-drying to make MXene-PEI-SA (MPA) composite. The adsorption process was performed by blending MPA into Cr(VI) or CR dispersion. Absorbencies were measured at 540 and 497 nm wavelength for Cr(VI) and CR, respectively.

Jun *et al.* [206] studied the adsorption capacity of selected dyes (Methylene blue (MB) and acid blue 80 (AB)) using MXene and Al-based metal-organic framework (MOF) as adsorbents. Herein, the authors did the adsorption test following diversified experimental conditions by mixing adsorbents (MXene and MOF) and adsorbates (MB and AB). After varied investigations, the authors concluded that both adsorbents demonstrated an electrostatic interaction mechanism for the adsorption of dyes (MB and AB). In another study, Cui *et al.* [207] studied MXene with biomimetic anchoring of Fe_3O_4 for the removal of organic dyes using the Fenton reaction. Herein, the authors contract MX-MNOs composite by MXene and Fe_3O_4 magnetic nanoparticles (MNPs). For that, they used MXene, $FeCl_3$, dopamine hydrochloride, and hydrazinium hydrate, and the pH was adjusted by NaOH solution. After stirring and centrifuging, the product was separated and washed with ethyl alcohol, and deionized water followed by freeze-drying. The catalytic test was done with the mingling of organic dye concentrations and MX-MNPs dispersion. pH was adjusted by NaOH and HCl. The mixed solutions were kept in stirring for 3 min to perform absorption-desorption equilibrium. H_2O_2 aqueous solution is used to lunch the degradation process. In degradation, 1 mL solution had been taken at 1 min intervals and put in a tube with 3 mL ethyl alcohol. This mixture was centrifuged, and the upper suspension was measured to identify organic dye concentrations in the solution.

On the other hand, Wang *et al.* [208] investigated MXene/carbon nanotubes/cotton fabrics for textile wastewater treatment by use of solar-driven interfacial water evaporation. Herein, the authors assembled L-b-L photothermal layer on cotton fabric. For that, they used cleaned cotton fabric immersed in MXene solution and rinsed with water to deposit a negatively charged MXene layer. Hydrogen bonding van der Waals force interactions, and physical adhesion formed between MXene and cotton fabric. Then, this sample was dipped into CNTs dispersion followed by rinsing with water to deposit a positively charged CNTs layer. Electrostatic interaction and hydrogen bonding adhesion forces obtained between MXene/CNTs composite. Additionally, Jun *et al.* [209] studied MXene as sonocatalyst to evaluate the ultrasonic (US) degradation of textile dyes. Herein, the authors used a US reactor to experiment. Specific conditions had been followed to do ultrasonic degradation of methylene blue (MB) and acid blue 80 (AB) dyes. To form synergetic indices, the discharge of dyes was studied under us only, MXene and US/MXene mixed process.

Table 3 and Table S2 (Supporting information) summarize the essence of these studies. Table 3 illustrates the prerequisite elements of MXene to remediate textile dye from wastewater along with treatment systems. The important findings are also tabulated. Most of the literature used diverse chemicals such as PA, DMSO, HCL, NaCl, NaOH, $K_2Cr_2O_7$, Na_2SO_4, $NaHCO_3$, PEI, SA, APTES, MNPs, $CaCl_2$, MOF, CNTs, $C_{13}H_{14}N_4O$, HA, TBA, ECH with MXene nanomaterials as well as dye adsorption technique used to treat dye from textile wastewater. And finally, almost all studies concluded that MXene performed excellently as an adsorbent to remediate dyes from wastewater. On the other hand, Table S2 depicts the mechanism conducted between the MXene and textile dyes during the adsorption process. Various mathematical models have been performed in these studies to obtain the actual data on the adsorption process; the adsorbent and adsorbate relations between them.

5.2. Interpretation of section 5.1

The newly introduced 2D MXene nanomaterials have a great prospect for the treatment of textile wastewater specifically to eliminate the dyes. In this current study, the conventional physiochemical strategy to remediate dyes has been upgraded by using MXene nanomaterials. The literature stated (Section 5.1) that chemical bonding and chemical composition play a supreme role in dye remediation. MXene performed diversified interactions with dye molecules as an adsorbent to separate it from wastewater as shown in Fig. 9. Herein, most of the studies inferred that electrostatic and ion exchange complexation interaction between MXene and dyes is the main mechanism to remediate dyes from wastewater. However, the literature stated other mechanisms also signify the remediation of dyes such as hydrogen interaction, surface charge, catalytic degradation, Fenton reaction, formation of free radicals, aggregation kinetic forces, diffusion rate, sonocatalyst degradation, chelation interaction, condensing, evaporation, and formation of active adsorption sites. Feng *et al.* [205] reported the possible mechanism of dye on MXene-based adsorbent as shown in Fig. 10. Herein, the electrostatic interaction occurred between the positively charged amino groups of MXene adsorbent and negatively charged dye ions. Also, hydrogen bonds formed be-

Fig. 9. Nine mechanisms occur during the adsorption process between MXene and textile wastewater treatment.

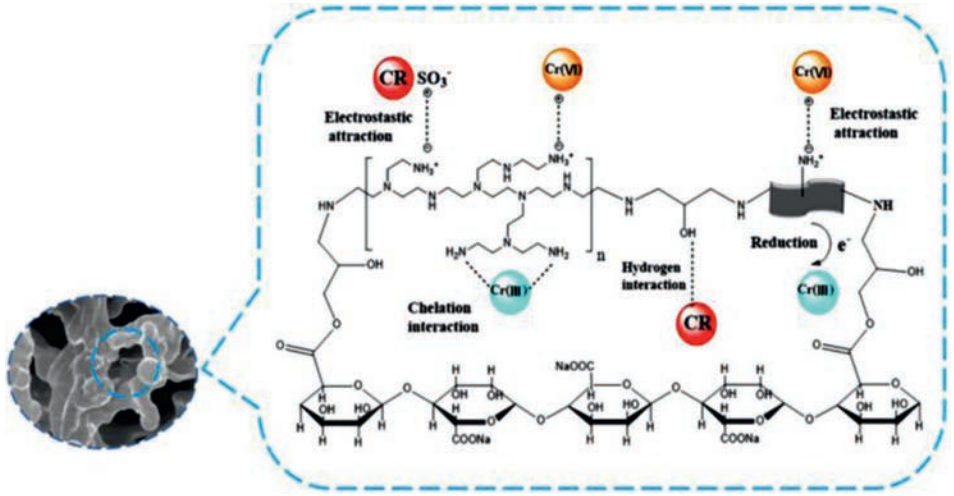

Fig. 10. Potential mechanism of dyes on MXene-based adsorbent. Adapted with permission [205]. Copyright 2021, Elsevier.

tween dye molecules and the MXene-based adsorbent. The produced dye molecules played the role to form a chelation reaction between produced dye molecules from the reaction of MXene with mother dye molecules and the MXene-based adsorbent. Also, Jun *et al.* [209] described the probable mechanism between dye molecules and MXene-based adsorbents as shown in Fig. 11. Herein, the US/MXene process portrayed good remediation of dyes (MB) due to distinct chemical reactions such as electrostatic attractions between dispersed MXene and due molecules, and the formation of hydroxyl radicals ($OH^{\cdot}$) to degrade the dyes; thus, enhancing the separation of dye from wastewater. Besides, a lot of influential significant parameters work in adsorption process that has been schematically presented in Fig. 12.

Influence of pH: pH has a significant effect on the adsorption performance of adsorbent and adsorbate [202] in the adsorption process. The removal rate of adsorbate and the equilibrium adsorption capacity of adsorbent is also influenced by pH [203]. The electrostatic effects such as electrostatic attraction, electrostatic repulsion, and isoelectric point dominate the pH in the adsorption process [206]. The ionic behavior of adsorbate and adsorbent is also effective on pH in the adsorption process [204,205,207,209].

Influence of adsorbent dose: Adsorption performance is associated with adsorbent dose in the adsorption process. The removal rate of dyes improved due to enhance in the adsorbent dose [205,206]. This happened to owe to an increase in the active adsorption sites on the surface of the adsorbent that depends on

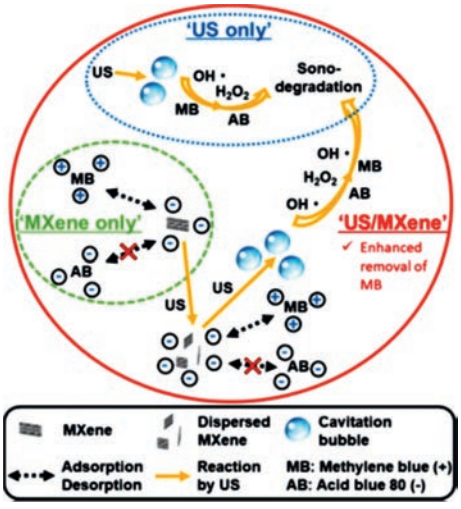

Fig. 11. Possible mechanism of dyes and MXene-based adsorbent. Adapted with permission [209]. Copyright 2021, Elsevier.

the degree of active adsorption sites on the amount of adsorbent and adsorbate in the adsorption process [202,203]. The comparably higher diffusion rate is also responsible for the active adsorption site leading to a great adsorption process [210].

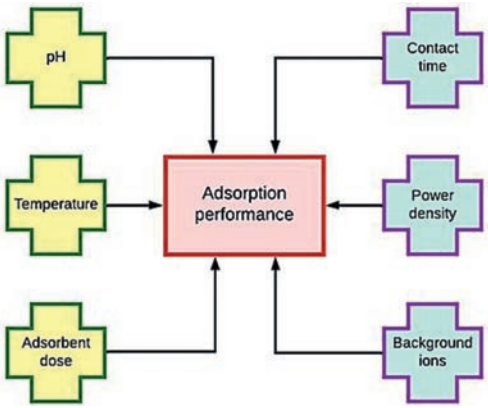

Fig. 12. Influential factors of adsorption performance during textile wastewater treatment.

Influence of temperature: Temperature is another important aspect affecting the adsorption performance in the adsorption process. Rising temperature enhances the active adsorption sites and diffusion rate which upgraded the adsorption performance. Adsorption is an endothermic process due to the development of temperature-increased adsorption capacity of adsorbate [203,211]. An increased temperature sometimes also improves vibrating intensity owning to adsorption-desorption actions of adsorbates from adsorbents in the adsorption process [202,212]. The dye removal rate lifted spontaneously by growing temperature in the solution [206].

Influence of contact time: The adsorption process is also time-based. The adsorption efficiency of adsorbate and adsorbent is fast in the primary phase. The synergistic response between adsorbent and adsorbate works more significantly and shows higher adsorption efficiency in the initial stage of the adsorption process. Numerous electrostatic effects such as electrostatic interaction, ion exchange, and complexation occurred on the surface of adsorbate and adsorbent during this process. After a certain period, the adsorption process reaches its saturation point, and no electrostatic effects are found after this point [203,204,206].

Influence of power density: Power density is another influential factor in the adsorption process. Increasing power density develops the growth rate of catalytic degradation action that enhances the adsorption performance of the adsorbent [206].

Influence of background ions: Background ions also affect the dye adsorption process by adsorbent significantly. Ionic strength and divalent cations/anions are the background ions of the adsorption process owing to electrostatic performance which is the predominant mechanism in the adsorption process [210]. Therefore, Jun *et al.* [206] showed that the ionic strength and divalent cation/anion influence the removal rate and adsorption equilibrium of dyes MXene and MXene-based adsorbents. In some cases, the removal rate and adsorption equilibrium decrease, and in other cases, it is increased by using MXene and MXene-based absorbent. High ionic strength can deplete the electrostatic attraction; therefore, declaim degrade the removal and adsorption equilibrium. Whereas also can sluggish the electrostatic repulsion force between dyes and adsorbents, thus enhancing the dye removal rate and adsorption equilibrium between adsorbate and adsorbent [213]. Besides, Jun *et al.* [206] reported that divalent count ions enhanced the dye removal rate and adsorption equilibrium of dyes. However, co-ions can decrease the adsorption performance as well.

Moreover, for a better practical understanding of the adsorption process, it is essential to analyze the adsorption isotherm equations. The adsorption efficiency can be determined accurately by adsorption isotherm mathematical expressions such as the Langmuir isotherm model [214] and the Freundlich isotherm model [215] (Table S2). The homogeneous and heterogeneous adsorption surfaces can be illustrated by Langmuir and Freundlich models respectively. A homogeneous surface defines equal affinities to the adsorbate [216]. MXene and MXene-based adsorbent demonstrated a better regression correlation coefficient in the Langmuir isotherm than the Freundlich isotherm model which signifies a homogeneous surface, which means homogeneity of adsorption active sites on MXene. Also, the MXene adsorbent performed the monolayer adsorption attribute. The homogeneous surface retains considerable active functional groups such as -OH, =O with varied binding forces on the MXene absorbent surface [202,204,205]. Moreover, to explain the degradation behavior of the adsorption process; classical kinetic models such as *pseudo*-first-order (PFO) and *pseudo*-second-order (PSO) kinetics models had been tailored with the observation of the adsorption process (Table S2). PFO and PSO models demonstrate the sorption kinetics of adsorbate onto the MXene which is determined by chemical forces between adsorbate and adsorbent [202,204,205]. MXene is suited more to the PSO model than PFO kinetic with experimental data which define that MXene is a chemically rate-controlled structure. Mass transfer, particle diffusion, and physiochemical attractions signify the structure of MXene [202,204].

Not only that, regeneration or reproducibility of adsorbent is an essential aspect for assessing the utilization from a practical feasibility standpoint [175]. Numerous studies reviewed that MXene and MXene-based composite exhibited superb reusability performance in the repeated adsorption process of dyes [202,203,206,209]. Herein, these experimental studies have done individual types of repeated adsorption tests of dyes with MXene nanomaterials. Literature reported that MXene and MXene-based composite performed excellent stability and reusability properties after repeated washing tests. For instance; Cai *et al.* [202] concluded that MXene-based composite demonstrated around 85% and 84% adsorption capacity after 12 continuous cycles for MB and RhB dyes respectively as shown in Figs. 13A and B.

Finally, after a critical review of the literature specifically in Sections 4.3 and 5.2, it has been stated that noble MXene nanomaterials are going to be the most auspicious nanomaterials in the textile field (both in smart textiles and textile wastewater treatment). In the case of smart textiles, MXene is characterized by various surface functional groups [217] and textile raw (Particularly fibers) possess chemically varied functional groups in their structure according to characteristics [218] which form diversified bonds between them to enhance the smart clothing performance. Not only that but also several actions work between MXene and textile raw materials such as van der Waals, adhesion, electrostatic interactions (Fig. 6). Herein, it has been observed that MXene nanomaterial is applied in three main forms of textile raw material such as fiber, yarn, and fabric form to produce advanced smart textile materials to heighten the performance of smart textiles. The next-generation clothing exhibited some outstanding results in application such as efficiency enhancement, increased sensing magnitude, improvement in capacitance, advancement of electrical conductivity, development of hydrophobicity, upgrade breathability, when MXene nanomaterials were incorporated into textile raw materials. On the other hand, most of the literature stated, that the adsorption process remediates dye molecules (adsorbate) from textile wastewater by using MXene (adsorbent). Diverse surface functional groups and surface charges of MXene make it prone to react with dye molecules of textile wastewater efficiently. Several mechanisms work between MXene and dye molecules such as electric interaction, kinetic forces, diffusion, chelating action (Fig. 9). To remediate textile dyes with MXene provide some unprecedented resultant data with adsorption capacity enhancement of dyes, developed dye molecules degradation as well as good catalytic behavior

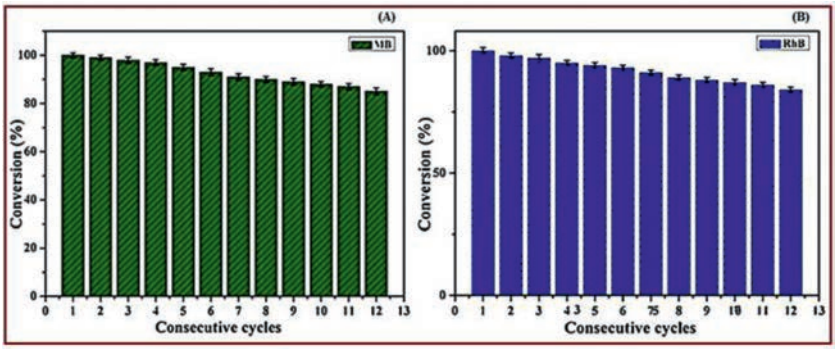

Fig. 13. Reusability performance of MXene in the adsorption process. Adapted with permission [202]. Copyright 2020, Elsevier.

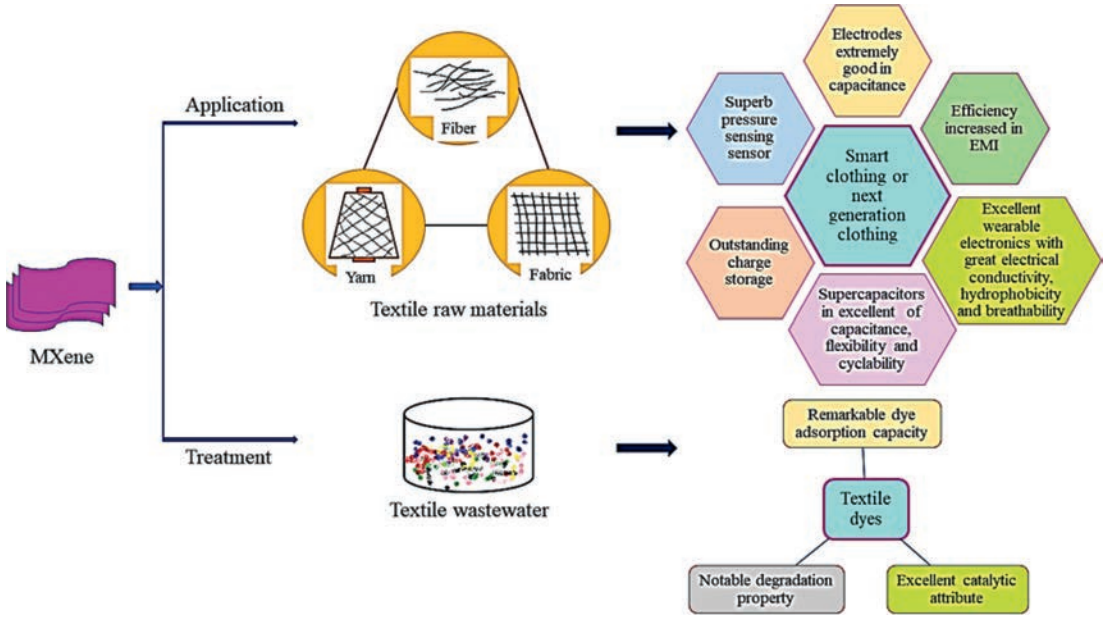

Fig. 14. Implementation and performance scenarios of MXene in smart textiles industries and wastewater remediation.

of dyes. The comprehensive scenario of the incorporation of MXene in textile materials has been demonstrated in Fig. 14.

6. Conclusion and challenges

The MXenes are the rustic competitor for the advancement of smart textiles performance and textile wastewater remediation. MXene-based textiles composites exhibited immense performance in smart textiles such as electrodes, supercapacitors, pressure sensors, and strain-sensing sensors for checking, monitoring, and evaluating the human body's response appropriately. There are enormous synthesis techniques that have been revealed to prepare a complex MXene-textile composite for smart textiles and these techniques have been illustrated here in a systematic way. Among them, the dip-coating approach has been used in most cases and presented phenomenal results in next-generation textiles. Furthermore, MXene depicted exceptional potential to treat textile dyes from wastewater by adsorption technique. To increase the adsorption effectiveness, several factors, such as solution pH, temperature, contact time, adsorbent dose, power density, and background ions, can affect the adsorption of textile dyes on MXene-based nanocomposites. Each dye, however, favors various physical and chemical adsorption conditions. It is concluded that nanocomposites based on MXene might be a great material for removing dyes from textile effluent. In this study, despite challenges, the recently developed scenario portrays promising results that have been figured out by researching the current studies. The present results demonstrate an enormous improvement in the application field of the textile sector which could be unique nanomaterials as anticipated in the upcoming days. Moreover, due to their large surface area, the higher number of surface functional groups with negatively charged, and solution processability, MXenes, a new family of two-dimensional (2D) materials, have shown to be promising candidates for producing functional fibers. They are also more suitable for creating smart textiles because of their exceptional electrical and electrochemical properties. Therefore, more research is imperative to affect the present obstacles surrounding with MXene for the application in textiles both in raw materials and wastewater treatment. The precious MXene has inaugurated a new era of nanomaterials that could be most significant in the textile field as well.

On the other hand, the unique idea of metal or nanoparticles used in textiles is an exceptional concept. The emergence of 2D transition metal carbide and nitride called "MXene" has revolutionized material chemistry research due to its unique properties such as metallic conductivity, rich surface chemistry, tunable terminations, and excellent processability. Whereas using MXene in textiles has some challenges both in research and commercial. One major challenge is the low yield and high cost of MXenes production. Currently, MXenes are produced at the lab scale with a small yield but developing an industrial-scale production process considering a cost-effective system is a great challenge that will

open the door to new applications in the new area. For large-scale production, the cost is predicted to be quite cheap. MXenes' potential as an adsorbent in continuous operation systems needs to be investigated. The traditional process for synthesizing MXenes, which involves the use of toxic hydrofluoric acid (HF, has been linked to major health and environmental concerns. The substitution of green or less harmful compounds for HF in the synthesis of MXene can ensure an environmentally friendly method. For the spinning process in textiles, MXene has a big scope but needs to innovate a spinning production line for MXene core yarn to overcome the challenge.

Declaration of competing interest

The authors declare that they have no known competing financial interests or personal relationships that could have appeared to influence the work reported in this paper.

Acknowledgments

The authors would like to thank the University Malaysia Pahang for the financial aid providing the grants (Nos. RDU 213308 and RDU 192207.

Supplementary materials

Supplementary material associated with this article can be found, in the online version, at doi:10.1016/j.cclet.2023.108533.

References

[1] S. Ramakrishna, R. Jose, Sci. Total Environ. 806 (2022) 151208.
[2] A. Fakharuddin, H. Li, F. Di Giacomo, et al., Adv. Energy Mater. 11 (2021) 2101443.
[3] Q. Huang, D. Wang, Z.J.A.E.M. Zheng, Adv. Energy Mater. 6 (2016) 1600783.
[4] K. Farhana, M. Syduzzaman, D. Yeasmin, J. Textile Sci. Technol. 5 (2015) 75–84.
[5] A. Şen, Int. J. Product. Econ. 114 (2008) 571–593.
[6] A. Maziz, A. Concas, A. Khaldi, et al., Sci. Adv. 3 (2017) e1600327.
[7] M. Stoppa, A.J. Chiolerio, Sensors 14 (2014) 11957–11992.
[8] M. Syduzzaman, S.U. Patwary, K. Farhana, et al., J. Textile Sci. Eng. 5 (2015) 1000181.
[9] L. Xue, W. Fan, Y. Yu, et al., Adv. Fiber Mater. 3 (2021) 239–250.
[10] K. Farhana, M. Syduzzaman, D. Yeasmin, J. Adv. Eng. Technol. 3 (2015) 1–7.
[11] D.P. Dubal, N.R. Chodankar, D.H. Kim, et al., Chem. Soc. Rev. 47 (2018) 2065–2129.
[12] K. Chaudhary, B. Kandasubramanian, Ind. Eng. Chem. Res. 61 (2022) 3789–3816.
[13] G. Chen, X. Xiao, X. Zhao, et al., Chem. Rev. 122 (2022) 3259–3291.
[14] S. Cho, T. Chang, T. Yu, et al., Biosensors 12 (2022) 222.
[15] A. Libanori, G. Chen, X. Zhao, et al., Nat. Electron. 5 (2022) 142–156.
[16] S. Ramakrishna, R. Jose, P.S. Archana, et al., J. Mater. Sci. 45 (2010) 6283–6312.
[17] A.M. Al-Dhahebi, J. Ling, S.G. Krishnan, et al., Appl. Phys. Rev. 9 (2022) 011319.
[18] A. Balilonda, Q. Li, X. Bian, et al., Chem. Eng. J. 410 (2021) 128384.
[19] A. Forouzan, M. Yousefzadeh, M. Latifi, et al., Macromol. Mater. Eng. 306 (2021) 2000510.
[20] J. Feng, E. Hontañón, M. Blanes, et al., ACS Appl. Mater. Interfaces 8 (2016) 14756–14765.
[21] H. Morris, R. Murray, Textile Progress 52 (2020) 1–127.
[22] M. Joshi, A. Bhattacharyya, Textile Progress 43 (2011) 155–233.
[23] F. De Falco, V. Guarino, G. Gentile, et al., J. Colloid Interf. Sci. 541 (2019) 367–375.
[24] T. Makowski, D. Kowalczyk, W. Fortuniak, et al., Cellulose 22 (2015) 3063–3075.
[25] L. Xie, B. Shan, H. Xu, et al., ACS Appl. Nano Mater. 1 (2018) 2406–2413.
[26] M.P. Gashti, E. Pakdel, F. Alimohammadi, Active Coatings for Smart Textiles, Elsevier, 2016, pp. 243–268.
[27] M. Joshi, B. Adak, Advances in nanotechnology based functional, smart and intelligent textiles: a review, Compr. Nanosci. Nanotechnol., 2nd ed., 2019.
[28] H. Yang, B. Yu, P. Song, et al., Compos. Part B: Eng. 176 (2019) 107185.
[29] U. Sharma, S. Karazhanov, R. Jose, et al., J. Mater. Chem. A 10 (2022) 8626–8655.
[30] H. Liu, K. Sun, X. Shi, et al., Energy Stor. Mater. 42 (2021) 845–870.
[31] Y. Feng, F. Zhou, Q. Deng, et al., Ceram. Int. 46 (2020) 8320–8327.
[32] F. Du, H. Tang, L. Pan, et al., Electrochim. Acta 235 (2017) 690–699.
[33] M. Naguib, V.N. Mochalin, M.W. Barsoum, et al., Adv. Mater. 26 (2014) 992–1005.
[34] D. Dhamodharan, V. Dhinakaran, H.S. Byun, Carbon 192 (2022) 366–383.
[35] M. Mozafari, M.J. Soroush, Mater. Adv. 2 (2021) 7277–7307.
[36] J. Azadmanjiri, T.N. Reddy, B. Khezri, et al., J. Mater. Chem. A 10 (2022) 4533–4557.
[37] M. Tomy, A. Ambika Rajappan, V. Vm, et al., Energy Fuels 35 (2021) 19881–19900.
[38] C. Couly, M. Alhabeb, K.L. Van Aken, et al., Adv. Electron. Mater. 4 (2018) 1700339.
[39] S. Li, L. Wang, J. Peng, et al., Chem. Eng. J. 366 (2019) 192–199.
[40] T.L. Tan, H.M. Jin, M.B. Sullivan, et al., ACS Nano 11 (2017) 4407–4418.
[41] A. Ahmed, M.M. Hossain, B. Adak, et al., Chem. Mater. 32 (2020) 10296–10320.
[42] K. Maleski, C.E. Ren, M.Q. Zhao, et al., ACS Appl. Mater. Interfaces 10 (2018) 24491–24498.
[43] A. Levitt, J. Zhang, G. Dion, et al., Adv. Funct. Mater. 30 (2020) 2000739.
[44] S. Uzun, S. Seyedin, A.L. Stoltzfus, et al., Adv. Funct. Mater. 29 (2019) 1905015.
[45] J. Zhang, N. Kong, S. Uzun, et al., Adv. Mater. 32 (2020) 2001093.
[46] K. Maleski, V.N. Mochalin, Y.J. Gogotsi, Chem. Mater. 29 (2017) 1632–1640.
[47] Q. Zhang, H. Lai, R. Fan, et al., ACS Nano 15 (2021) 5249–5262.
[48] X. Sui, Z. Yuan, Y. Yu, et al., Small 16 (2020) 2003400.
[49] V. Natu, M. Sokol, L. Verger, et al., J. Phys. Chem. C 122 (2018) 27745–27753.
[50] J. Orangi, F. Hamade, V.A. Davis, et al., ACS Nano 14 (2019) 640–650.
[51] L. Liu, R. Guo, J. Gao, et al., Compos. Commun. 30 (2022) 101094.
[52] S. Ramakrishna, R. Jose, Matter 5 (2022) 4097–4099.
[53] J. Yin, F. Zhan, T. Jiao, et al., Chin. Chem. Lett. 31 (2020) 992–995.
[54] K. Li, T. Jiao, R. Xing, et al., Sci. China Mater. 61 (2018) 728–736.
[55] L. Damptey, B.N. Jaato, C.S. Ribeiro, et al., Glob. Challenges 6 (2022) 2100120.
[56] G. Zeng, K. Wei, H. Zhang, et al., Appl. Clay Sci. 211 (2021) 106177.
[57] M. Ahmaruzzaman, RSC Adv. 12 (2022) 34766–34789.
[58] H. Assad, I. Fatma, A. Kumar, et al., Chemosphere (2022) 134221.
[59] M. Ahmaruzzaman, Inorg. Chem. Commun. 143 (2022) 109705.
[60] M. Jeon, B.-M. Jun, S. Kim, et al., Chemosphere 261 (2020) 127781.
[61] Y. Ibrahim, A. Kassab, K. Eid, et al., Nanomaterials 10 (2020) 885.
[62] Y. Li, R. Dai, H. Zhou, et al., ACS Appl. Nano Mater. 4 (2021) 6328–6336.
[63] X. Wu, M. Ding, H. Xu, et al., ACS Nano 14 (2020) 9125–9135.
[64] Y. Ibrahim, M. Meslam, K. Eid, et al., Sep. Purif. Technol. 282 (2022) 120083.
[65] H. Lei, Z. Hao, K. Chen, et al., J. Phys. Chem. Lett. 11 (2020) 4253–4260.
[66] N. Hemanth, B.J. Kandasubramanian, Chem. Eng. J. 392 (2020) 123678.
[67] M. Naguib, M. Kurtoglu, V. Presser, et al., Adv. Mater. 23 (2011) 4248–4253.
[68] P.O. Persson, J. Rosen, Curr. Opin. Solid State Mater. Sci. 23 (2019) 100774.
[69] A. Sarycheva, Y. Gogotsi, Chem. Mater. 32 (2020) 3480–3488.
[70] M.W. Barsoum, M. Radovic, Ann. Rev. Mater. Res. 41 (2011) 195–227.
[71] B. Anasori, M.R. Lukatskaya, Y.J. Gogotsi, Nat. Rev. Mater. 2 (2017) 1–17.
[72] A. Sreedhar, J.S.J. Noh, Solar Energy 222 (2021) 48–73.
[73] M. Magnuson, M. Mattesini, Thin Solid Films 621 (2017) 108–130.
[74] F. Jamil, H.M. Ali, M.M.J. Janjua, J. Energy Storage 35 (2021) 102322.
[75] M. Alhabeb, K. Maleski, B. Anasori, et al., Chem. Mater. 29 (2017) 7633–7644.
[76] M. Sajid, Anal. Chim. Acta 1143 (2021) 267–280.
[77] X. Zhan, C. Si, J. Zhou, et al., Nanoscale Horiz. 5 (2020) 235–258.
[78] O. Mashtalir, M. Naguib, V.N. Mochalin, et al., Nat. Commun. 4 (2013) 1716.
[79] L. Verger, C. Xu, V. Natu, et al., Curr. Opin. Solid State Mater. Sci. 23 (2019) 149–163.
[80] J. Halim, S. Kota, M.R. Lukatskaya, et al., Adv. Funct. Mater. 26 (2016) 3118–3127.
[81] O. Salim, K. Mahmoud, K. Pant, et al., Mater. Today Chem. 14 (2019) 100191.
[82] Y. Li, H. Shao, Z. Lin, et al., Nat. Mater. 19 (2020) 894–899.
[83] Q. Xu, S. Chen, J. Xu, et al., J. Electroanal. Chem. 880 (2021) 114765.
[84] Y. Liu, J. Yu, D. Guo, et al., J. Alloys Compd. 815 (2020) 152403.
[85] C. Prasad, X. Yang, Q. Liu, et al., J. Indust. Eng. Chem. 85 (2020) 1–33.
[86] S. Jolly, M.P. Paranthaman, M. Naguib, Mater. Today Adv. 10 (2021) 100139.
[87] A. Tanvir, P. Sobolčiak, A. Popelka, et al., Polymers 11 (2019) 1272.
[88] M. Ghidiu, M.R. Lukatskaya, M.Q. Zhao, et al., Nature 516 (2014) 78–81.
[89] J. Yin, K. Wei, J. Zhang, et al., Cell Rep. Phys. Sci. 3 (2022) 100893.
[90] A. Lipatov, M. Alhabeb, M.R. Lukatskaya, et al., Adv. Electron. Mater. 2 (2016) 1600255.
[91] H. Wang, Y. Wu, J. Zhang, et al., Mater. Lett. 160 (2015) 537–540.
[92] A.S. Zeraati, S.A. Mirkhani, P. Sun, et al., Nanoscale 13 (2021) 3572–3580.
[93] M. Hu, H. Zhang, T. Hu, et al., Chem. Soc. Rev. 49 (2020) 6666–6693.
[94] R. Ma, Z. Chen, D. Zhao, et al., J. Mater. Chem. A 9 (2021) 11501–11529.
[95] Q. Zhu, J. Li, P. Simon, et al., Energy Stor. Mater. 35 (2021) 630–660.
[96] L. Li, D. Zhang, J. Deng, et al., Sustain. Energy Fuels 5 (2021) 3278–3291.
[97] W. Meng, X. Liu, H. Song, et al., Nano Today 40 (2021) 101273.
[98] J. Nan, X. Guo, J. Xiao, et al., Small 17 (2021) 1902085.
[99] K. Nasrin, V. Sudharshan, K. Subramani, et al., Adv. Funct. Mater. 32 (2022) 2110267.
[100] A.M. Al-Dhahebi, R. Jose, M. Mustapha, et al., Food Chem. 390 (2022) 133105.
[101] X. Wang, X. Wang, J. Yin, et al., Compos. Part B: Eng. 241 (2022) 110052.
[102] J. Pang, R.G. Mendes, A. Bachmatiuk, et al., Chem. Soc. Rev. 48 (2019) 72–133.
[103] Q. Zhang, Z. Tian, P. Zhang, et al., Mater. Today Commun. 31 (2022) 103466.
[104] Y. Bai, K. Zhou, N. Srikanth, et al., RSC Adv. 6 (2016) 35731–35739.
[105] M. Naguib, T. Saito, S. Lai, et al., RSC Adv. 6 (2016) 72069–72073.
[106] I. Persson, L.Å. Näslund, J. Halim, et al., 2D Mater. 5 (2017) 015002.
[107] Z. Fu, H. Zhang, C. Si, et al., J. Phys. Chem. C 122 (2018) 4710–4722.
[108] V.N. Borysiuk, V.N. Mochalin, Y. Gogotsi, Nanotechnology 26 (2015) 265705.
[109] S. Lu, W. Ren, J. He, et al., Phys. Rev. B 105 (2022) 165301.
[110] A. Lipatov, H. Lu, M. Alhabeb, et al., Sci. Adv. 4 (2018) eaat0491.

[111] Y. Zhou, K. Maleski, B. Anasori, et al., ACS Nano 14 (2020) 3576–3586.
[112] Y. Dai, X. Wu, L. Li, et al., J. Mater. Chem. A 10 (2022) 11375–11385.
[113] A. Ahmed, S. Sharma, B. Adak, et al., InfoMat 4 (2022) e12295.
[114] Z. Fan, Y. Yang, H. Ma, et al., Carbon 186 (2022) 150–159.
[115] F.H. Saboor, S. Hadian-Gazvini, S. Shahsavari, Applications of carbon-based conductive nanomaterials on e-textiles, in: Nanosensors and Nanodevices for Smart Multifunctional Textiles, Elsevier, 2021, pp. 245–265.
[116] M.O. Faruk, A. Ahmed, M.A. Jalil, et al., Appl. Mater. Today 23 (2021) 101025.
[117] Z. Zhang, H. Cao, Y. Quan, et al., Polymers 14 (2022) 1213.
[118] A. Bhat, S. Anwer, K.S. Bhat, et al., NPJ 2D Mater. Appl. 5 (2021) 1–21.
[119] A. Levitt, D. Hegh, P. Phillips, et al., Mater. Today 34 (2020) 17–29.
[120] S. Qin, K.A.S. Usman, D. Hegh, et al., ACS Appl. Mater. Interfaces 13 (2021) 36655–36669.
[121] Z. Guo, Y. Li, Z. Lu, W. Liu, J. Phys.: Conf. Ser. 1790 (2021) 012066.
[122] Z. Wu, L. Wei, S. Tang, et al., ACS Nano 15 (2021) 18880–18894.
[123] S. Uzun, M. Schelling, K. Hantanasirisakul, et al., Small 17 (2021) 2006376.
[124] Z. Ling, C.E. Ren, M.Q. Zhao, et al., Proc. Natl. Acad. Sci. U. S. A. 111 (2014) 16676–16681.
[125] M. Pourmohammad, J. Ling, M. Yousefzadeh, et al., Energy Fuels 36 (2022) 15268–15278.
[126] K. Singha, J. Kumar, P.J. Pandit, Mater. Today: Proc. 16 (2019) 1518–1523.
[127] G. Cho, S. Lee, J. Cho, Int. J. Hum.-Comput. Interact. 25 (2009) 582–617.
[128] T. Takagi, J. Intell. Mater. Syst. Struct. 1 (1990) 149–156.
[129] D.C. Çelikel, Smart e-textile materials, in: N. Tasaltin, P.S. Nnamchi, S. Saud (Eds.), Advanced Functional Materials Eds., IntechOpen, 2020, pp. 1–16, doi:10.5772/intechopen.92439.
[130] G. Stylios, Assemb. Autom. 16 (1996) 40–44.
[131] R.B. Katragadda, Y. Xu, Sens. Actuators A: Phys. 143 (2008) 169–174.
[132] S. Arora, A. Ghosh, Evolution of soft body armor, in: S. Ul-Islam, B.S. Butola (Eds.), Advanced Textile Engineering Materials, John Wiley & Sons, 2018, pp. 499–541.
[133] M. Joshi, A. Bhattacharyya, S.W. Ali, Indian J. Fibre Textile Res. 33 (2008) 304–317.
[134] B. Pal, J.B. Matsoso, A.K. Parameswaran, et al., Electrochim. Acta 415 (2022) 140239.
[135] K. Cherenack, K. Van OS, L. Van Pieterson, Photonics applied: wearable photonics: smart photonic textiles begin to weave their magic, Laser Focus world, 2012.
[136] A.K. Yetisen, H. Qu, A. Manbachi, et al., ACS Nano 10 (2016) 3042–3068.
[137] B.H. Dong, J.P. Hinestroza, ACS Appl. Mater. Interfaces 1 (2009) 797–803.
[138] H. Esmaeilzadeh, M. Rivard, E. Arzi, et al., Opt. Express 23 (2015) 14981–14992.
[139] J. Hu, H. Meng, G. Li, et al., Smart Mater. Struct. 21 (2012) 053001.
[140] M. Cinquino, C.T. Prontera, M. Pugliese, et al., Micromachines 12 (2021) 652.
[141] A. Lendlein, S.J. Kelch, Angew. Chem. Int. Ed. 41 (2002) 2034–2057.
[142] S. Mondal, Appl. Thermal Eng. 28 (2008) 1536–1550.
[143] C. Kaviarasu, D.J. Prakash, J. Eng. Sci. Technol. Rev. 9 (2016) 26–36.
[144] L.M. Castano, A.B. Flatau, Smart Mater. Struct. 23 (2014) 053001.
[145] M. Yousaf, H.T.H. Shi, Y. Wang, et al., Adv. Energy Mater. 6 (2016) 1600490.
[146] J. Tabor, K. Chatterjee, T.K. Ghosh, Adv. Mater. Technol. 5 (2020) 1901155.
[147] S. Pan, H. Lin, J. Deng, et al., Adv. Energy Mater. 5 (2015) 1401438.
[148] V. Koncar, Introduction to smart textiles and their applications, Smart Textiles and Their Applications, Elsevier, 2016, pp. 1–8.
[149] S.S. Shah, M.N. Shaikh, M.Y. Khan, et al., Chem. Rec. 21 (2021) 1631–1665.
[150] T. Li, L. Chen, X. Yang, et al., J. Mater. Chem. C 7 (2019) 1022–1027.
[151] J. Yan, Y. Ma, C. Zhang, et al., RSC Adv. 8 (2018) 39742–39748.
[152] X. Zheng, W. Nie, Q. Hu, et al., Mater. Design 200 (2021) 109442.
[153] G. Yin, Y. Wang, W. Wang, et al., Colloids Surf. A: Physicochem. Eng. Aspects 601 (2020) 125047.
[154] S. Wang, X. Du, Y. Luo, et al., Chem. Eng. J. 408 (2021) 127363.
[155] W.T. Cao, C. Ma, D.S. Mao, et al., Adv. Funct. Mater. 29 (2019) 1905898.
[156] L.X. Liu, W. Chen, H.B. Zhang, et al., Adv. Funct. Mater. 29 (2019) 1905197.
[157] M. Hu, T. Hu, R. Cheng, et al., J. Energy Chem. 27 (2018) 161–166.
[158] X. Li, J. Hao, R. Liu, et al., Energy Storage Mater. 33 (2020) 62–70.
[159] W. Shao, M. Tebyetekerwa, I. Marriam, et al., J. Power Sources 396 (2018) 683–690.
[160] Q.W. Wang, H.B. Zhang, J. Liu, et al., Adv. Funct. Mater. 29 (2019) 1806819.
[161] L. Wang, M. Tian, Y. Zhang, et al., J. Mater. Sci. 55 (2020) 6187–6194.
[162] S. Seyedin, S. Uzun, A. Levitt, et al., Adv. Funct. Mater. 30 (2020) 1910504.
[163] J. Luo, S. Gao, H. Luo, et al., Chem. Eng. J. 406 (2021) 126898.
[164] W. He, M. Sohn, R. Ma, et al., Nano Energy 78 (2020) 105383.
[165] I. Ihsanullah, A. Jamal, M. Ilyas, et al., J. Water Process Eng. 38 (2020) 101680.
[166] N.Y. Donkadokula, A.K. Kola, I. Naz, et al., Rev. Environ. Sci. Bio/Technol. 19 (2020) 543–560.
[167] B. Shi, G. Li, D. Wang, et al., J. Hazard. Mater. 143 (2007) 567–574.
[168] C. Yang, W. Xu, Y. Nan, et al., J. Colloid Interf. Sci. 562 (2020) 589–597.
[169] I. Arslan, I.J. Balcioglu, Dyes Pigments 47 (2000) 207–218.
[170] X. Quan, C. Ye, Y. Xiong, et al., J. Hazard. Mater. 178 (2010) 326–332.
[171] S. Karcher, A. Kornmüller, M.J. Jekel, Water Res. 36 (2002) 4717–4724.
[172] H.D. Raval, P.S. Rana, S. Maiti, RSC Adv. 5 (2015) 6687–6694.
[173] A. Regti, M.R. Laamari, S.E. Stiriba, et al., J. Assoc. Arab Univ. Basic Appl. Sci. 24 (2017) 10–18.
[174] S. Rajendra, M. Khan, F. Gracia, et al., Sci. Rep. 6 (2016) 31641.
[175] J. Han, B.M. Jun, J. Heo, et al., Ceram. Int. 45 (2019) 19247–19256.
[176] X.W. Liu, H.Q. Yu, B.J. Ni, G.P. Sheng, Adv. Biochem. Eng. Biotechnol. 113 (2009) 275–303.
[177] F.A. Al-Khaldi, B. Abusharkh, M. Khaled, et al., J. Mol. Liquids 204 (2015) 255–263.
[178] N.I. Blaisi, M. Zubair, S. Ali, et al., Environ. Sci. Pollut. Res. 25 (2018) 34319–34331.
[179] I. Ali, I. Burakova, E. Galunin, et al., ACS Omega 4 (2019) 19293–19306.
[180] R. Kishor, D. Purchase, G.D. Saratale, et al., J. Environ. Chem. Eng. 9 (2021) 105012.
[181] K. Rasool, R.P. Pandey, P.A. Rasheed, et al., Mater. Today 30 (2019) 80–102.
[182] O. Mashtalir, K.M. Cook, V.N. Mochalin, et al., J. Mater. Chem. A 2 (2014) 14334–14338.
[183] Y. Jin, Y. Fan, X. Meng, et al., Processes 7 (2019) 751.
[184] Y. Xia, T.S. Mathis, M.Q. Zhao, et al., Nature 557 (2018) 409–412.
[185] A.S. Levitt, M. Alhabeb, C.B. Hatter, et al., J. Mater. Chem. A 7 (2019) 269–277.
[186] R. Rashid, I. Shafiq, P. Akhter, et al., Environ. Sci. Pollut. Res. 28 (2021) 9050–9066.
[187] E. Şayan, Chem. Eng. J. 119 (2006) 175–181.
[188] L. Niazi, A. Lashanizadegan, H.J. Sharififard, J. Clean. Prod. 185 (2018) 554–561.
[189] Y. Yang, J. Yang, Y. Du, et al., ACS Omega 4 (2019) 17741–17751.
[190] K. Vikrant, B.S. Giri, N. Raza, et al., Bioresource Technol. 253 (2018) 355–367.
[191] M. Kaur, N. Kaur, K. Jeet, et al., Ceram. Int. 41 (2015) 13739–13750.
[192] A. Ayati, M.N. Shahrak, B. Tanhaei, et al., Chemosphere 160 (2016) 30–44.
[193] I. Ihsanullah, Chem. Eng. J. 388 (2020) 124340.
[194] M.M. Tunesi, R.A. Soomro, X. Han, et al., Nano Converg. 8 (2021) 1–19.
[195] N.A. Bakar, N. Othman, Z.M. Yunus, et al., Environ. Technol. Innovat. 22 (2021) 101445.
[196] O. Agboola, O.S.I. Fayomi, A. Ayodeji, et al., Membranes 11 (2021) 139.
[197] Y. Dong, D. Sang, C. He, et al., RSC Adv. 9 (2019) 29015–29022.
[198] A. Kong, Y. Sun, M. Peng, et al., Colloids Surf. A: Physicochem. Eng. Aspects 617 (2021) 126388.
[199] A. Shahzad, K. Rasool, W. Miran, et al., J. Hazard. Mater. 344 (2018) 811–818.
[200] K.N. Zhang, C.Z. Wang, Q.F. Lü, et al., Int. J. Biol. Macromol. 209 (2022) 680–691.
[201] B.M. Jun, C.M. Park, J. Heo, et al., J. Environ. Manag. 256 (2020) 109940.
[202] C. Cai, R. Wang, S. Liu, et al., Colloids Surf. A: Physicochem. Eng. Aspects 589 (2020) 124468.
[203] B.M. Jun, S. Kim, H. Rho, et al., Chemosphere 254 (2020) 126827.
[204] P. Karthikeyan, K. Ramkumar, K. Pandi, et al., Ceram. Int. 47 (2021) 3692–3698.
[205] Y. Feng, H. Wang, J. Xu, et al., J. Hazard. Mater. 416 (2021) 125777.
[206] B.M. Jun, J. Heo, N. Taheri-Qazvini, et al., Ceram. Int. 46 (2020) 2960–2968.
[207] Y. Cui, D. Zhang, K. Shen, et al., J. Environ. Chem. Eng. 8 (2020) 104369.
[208] Y. Wang, Q. Qi, J. Fan, et al., Sep. Purif. Technol. 254 (2021) 117615.
[209] B.M. Jun, J. Han, C.M. Park, et al., Ultrason. Sonochem. 64 (2020) 104993.
[210] B.M. Jun, S. Kim, Y. Kim, et al., Chemosphere 231 (2019) 82–92.
[211] S.M. Mirsoleimani-azizi, P. Setoodeh, S. Zeinali, et al., J. Environ. Chem. Eng. 6 (2018) 6118–6130.
[212] Y. Qu, C. Zhang, F. Li, et al., J. Hazard. Mater. 169 (2009) 146–152.
[213] K.T. Wong, Y. Yoon, S.A. Snyder, et al., Chemosphere 152 (2016) 71–80.
[214] I. Langmuir, J. Am. Chem. Soc. 38 (1916) 2221–2295.
[215] H. Freundlich, J. Phys. Chem. 57 (1906) 1100–1107.
[216] T. Sheela, Y.A.J. Nayaka, Chem. Eng. J. 191 (2012) 123–131.
[217] Y. Wu, X. Li, H. Zhao, et al., Chem. Eng. J. 418 (2021) 129296.
[218] S. Benkhaya, S. M'rabet, A. El Harfi, Inorg. Chem. Commun. 115 (2020) 107891.